From {$Au^{I}\cdots Au^{I}$}-Coupled Cages to the Cage-Built 2-D {$Au^{I}\cdots Au^{I}$} arrays: $Au^{I}\cdots Au^{I}$ Bonding Interaction Driven Self-Assembly and Their Ag^{I} Sensing and Photo-Switchable Behavior

Xuan-Feng Jiang[†], Franky Ka-Wah Hau[‡], Qing-Fu Sun[§], Shu-Yan Yu*[†,‖], Vivian Wing-Wah Yam*[‡]

[†]*Laboratory for Self-Assembly Chemistry, Department of Chemistry, Renmin University of China, Beijing 100872, P.R. China*
E-mail: yusy@ruc.edu.cn;

[‡]*Institute of Molecular Functional Materials (Areas of Excellence Scheme, University Grants Committee (Hong Kong)) and Department of Chemistry, The University of Hong Kong, Pokfulam Road, Hong Kong, P.R. China*
E-mail: wwyam@hku.hk

[§]*State Key Laboratory of Structural Chemistry, Fujian Institute of Research on the Structure of Matter, Chinese Academy of Sciences, Fuzhou 350002, P.R. China*

[‖]*Department of Chemistry and Chemical Industry, College of Environmental and Energy Engineering, Beijing University of Technology, Beijing 100124, P.R. China*

Supporting Information

Contents

S1. Materials and instrumentation

All reactions and manipulations were carried out under an atmosphere of prepurified nitrogen using Schlenk techniques. All the organic solvents were distilled over 4 Å molecular sieves under an argon atmosphere. All other chemicals were used as received without further purification. The ^{1}H NMR spectra of all compounds were recorded at 400 MHz on a Bruker AIVEN400 spectrometer. Halogenated and aromatic NMR solvents were dried over anhydrous potassium carbonate prior to use. The MALDI-TOF mass spectral analyses were carried out on a Bruker BIFLEX III spectrometer. The X-ray diffraction single-crystal data of **1–3** were collected at the Beijing Synchrotron Radiation Facility (BSRF).

S2. Experimental procedures

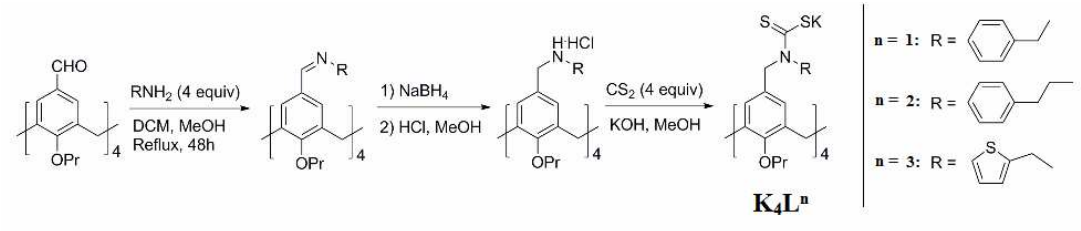

Scheme S1. Synthetic routes of tetrakis(4-carbodithiolatelphenyl) calix[4]arene ligand **$(L^1)K_4$, $(L^2)K_4$** and **(L^3) K_4**.

Synthesis and characterization of ligands:

5,11,17,23-tetraformyl-25,26,27,28-tetrapropoxycalix[4]arene was prepared according to a literature procedure.[1] The detailed synthesis of other ligands were made according to those of similar compounds reported in previous literatures.[2]

5,11,17,23-Tetra-(*N*-(phenylmethyl)-methanimine)-25,26,27,28-tetrapropoxy-calix[4]arene (calix-phenylmethyl-imine)

5,11,17,23-Tetraformyl-25,26,27,28-tetrapropoxycalix[4]arene (144.0 mg, 0.2 mmol) was added to a solution of benzylamine (91.0 mg, 0.85 mmol) in anhydrous methanol (10.0 mL) and dichloromethane (10.0 mL). The mixture was refluxed under an argon atmosphere for 24 h. The solution was then cooled and concentrated. Crystallization of the residue from CH_3OH afforded the target compound (Yield: 190 mg, 87 %) as a white solid. m.p. 250–260 ºC. ^{1}H NMR (400 MHz, $CDCl_3$, 298 K): δ = 7.90 (s, 4H, HC=N–), 7.28-7.31 (t, 8H, *J* = 8.2 Hz, Ar–C–N), 7.21 (d, *J* = 8.2 Hz, 8H, Ar–C–N), 7.13 (s, 8H, Ar–C=N), 4.59 (s, 8H, Ar–CH_2–N), 4.44, 3.24 (d, 8H, *J* = 13.2 Hz,

Ar–CH_2–Ar), 3.98 (t, 8H, *J* = 7.4 Hz, CH_3CH_2*CH_2*–O–Ar), 1.98 (ψ-sext, 8H, CH_3*CH_2*CH_2–O–Ar), 1.01 (t, 12H, *J* = 7.4 Hz, *CH_3*CH_2CH_2O). ^{13}C NMR (100 MHz, $CDCl_3$, 298 K, ppm): δ 162.04, 159.10, 139.81, 135.21, 134.96, 130.43, 129.58, 129.07, 128.43, 128.32, 128.05, 127.17, 127.17, 126.79, 125.39, 64.39, 23.11, 21.49, 10.34. IR (KBr, ν / cm^{-1}): 1623 (C=N), 1467 (Ar–H), 686 (C–H). MALDI-TOF-MS (CH_3OH) m/z: $[M + H_2O + K]^+$, calcd for $C_{72}H_{79}N_4O_5K^+$, 1117.56; found, 1117.6. Elemental analyses calcd (%) for $C_{73}H_{80}N_4O_5$•CH_3OH: C, 80.19; H, 7.37; N, 5.12. Found: C, 79.98; H, 7.29; N, 5.08.

5,11,17,23-Tetra-(*N*-(phenylethyl)-methanimine)-25,26,27,28-tetrapropoxy-calix[4]arene (calix-phenylethyl-imine)

5,11,17,23-Tetraformyl-25,26,27,28-tetrapropoxycalix[4]arene (195 mg, 0.27 mmol) was added to a solution of phenethylamine (113 mg, 0.95 mmol) in anhydrous toluene (30.0 mL). The mixture was refluxed under an argon atmosphere for 24 h. The light-yellow solution was cooled and concentrated under vacuum, and the crude residue was crystallized from CH_3OH affording the target compound (Yield: 265 mg, 85 %) as a white crystal, which was used without further purification in the next step. m.p. 250–260 ºC. ^{1}H NMR (400 MHz, $CDCl_3$, 298 K): δ = 7.96 (s, 4H, HC=N–), 7.53–7.39 (m, 28H, Ar–C–N), 4.69 and 3.49 (d, 8H, *J* = 7.6 Hz, Ar–CH_2–Ar), 4.12, (t, 8H, *J* = 7.2, Ar–CH_2–*CH_2*–N), 3.90 (t, 8H, *J* = 7.6 Hz, CH_3CH_2*CH_2*O–Ar), 3.14 (t, 8H, *J* = 7.2, Ar–*CH_2*–CH_2–N), 2.15 (ψ-sext, 8H, CH_3*CH_2*CH_2O–Ar), 1.23 (t, 12H, *J* = 7.2 Hz, *CH_3*CH_2CH_2O). ^{13}C NMR (100 MHz, $CDCl_3$, 298 K, ppm): δ 162.04, 159.10,

140.10, 135.12, 129.03, 128.96, 128.50, 128.38, 128.33, 126.10, 126.01, 62.944, 33.70, 30.92, 23.34, 10.30. IR (KBr, ν / cm^{-1}): 1627 (C=N), 1432 (Ar–H), 689 (C–H). MALDI-TOF-MS (CH_3OH) m/z: $[M + CH_3OH + Na]^+$, 1187.65; found, 1186.7. Elemental analyses calcd (%) for $C_{77}H_{86}Cl_2N_4O_4 \bullet CH_2Cl_2$: C, 76.91; H, 7.21; N, 4.66. Found: C, 76.83; H, 7.12; N, 4.57.

5,11,17,23-Tetra-(*N*-thienylmethyl-methanimine)-25,26,27,28-tetrapropoxy-calix[4]arene (calix-thienylmethyl-imine)

5,11,17,23-Tetraformyl-25,26,27,28-tetrapropoxycalix[4]arene (195 mg, 0.27 mmol) was added to a solution of 2-(2-Thienyl)ethylamine (95 mg, 0.95 mmol) in anhydrous toluene (30.0 mL). The mixture was refluxed under an argon atmosphere for 24 h. The light-yellow solution was cooled and concentrated under vacuum, and the crude residue was crystallized from CH_3OH affording the target compound (Yield: 235 mg, 81 %) as a white crystal, which was used without further purification in the next step. m.p. 230–240 ºC. ^{1}H NMR (400 MHz, $CDCl_3$, 298 K): δ = 7.89 (s, 4H, HC=N–), 7.28 (d, 4H, *J* = 8.2 Hz, thienyl-H), 6.99 (m, 4H, J = 8.4 Hz, thienyl-H), 6.90 (d, 4H, *J* = 8.2 Hz, thienyl-H), 7.19 (s, 8H, Ar–H), 4.77 (s, 8H, thienyl-CH_2–N), 4.46, 3.26 (d, 4H, *J* = 13.5 Hz, Ar–CH_2–Ar), 3.91 (s, 8H, Ar–O–CH_2), 1.95 (ψ-sext, 8H, $CH_3CH_2CH_2O$–Ar), 1.08 (t, 12H, *J* = 7.4 Hz, $CH_3CH_2CH_2O$–Ar). ^{13}C NMR (100 MHz, $CDCl_3$, 298 K, ppm): δ 162.28, 159.18, 142.96, 135.16, 130.22, 128.65, 126.80, 124.34, 124.23, 59.13, 30.84, 23.28, 10.32. IR (KBr, ν / cm^{-1}): 1619(C=N), 1438 (Ar–H), 1304 (C=S), 689(C–H). MALDI-TOF-MS (CH_3OH) m/z: $[M + H]^+$,

calcd for $C_{64}H_{67}N_4O_4S_4^+$, 1085.51; found, 1085.4. Elemental analyses calcd (%) for $C_{64}H_{72}N_4O_6S_4$•$2H_2O$: C, 68.54; H, 6.47; N, 5.00. Found: C, 69.05; H, 6.47; N, 5.08.

5,11,17,23-Tetra-(*N*-phenylmethyl-*N*-methyleneamine)-25,26,27,28-tetrapropoxy-calix[4]arene (calix-phenylmethyl-amine)

An excess of solid $NaBH_4$ (576.0 mg) was added to 5,11,17,23-tetra-(*N*-(phenylmethyl)-methanimine)-25,26,27,28-tetrapropoxycalix[4]-arene (180 mg) in CH_3OH in a nitrogen atmosphere at −5 ºC and stirred for 6 h. The mixture was then refluxed at 85 ºC overnight and evaporated to dryness, neutralized with aqueous 2 M HCl (30 mL) and extracted with CH_2Cl_2, (3 × 40 mL). The organic layer was separated, washed with H_2O (2 × 15 mL), dried over anhydrous Na_2SO_4, and the filtrate was evaporated to give a yellow oil. Concentrated aqueous HCl solution (36%, 12 mol/l) was added to obtained the target compound (Yield: 189 mg, 83 %) as a white solid. m.p. 227–230 ºC. ^{1}H NMR (400 MHz, DMSO-d_6, 298 K): δ = 9.61 (s, 8H, HCl·HN–C), 7.47 (s, 8H, *Ar*–CH_2N), 7.37 (d, 8H, *J* = 7.2 Hz, *Ar*–CH_2N), 7.10 (s, 8H, *Ar*–CH_2N), 4.35 (d, 8H, *J* = 12.8 Hz, Ar–*CH_2*–Ar), 3.19 (d, 8H, *J* = 12.8 Hz, Ar–*CH_2*–Ar), 3.99 (s, 8H, Ar–*CH_2*–N), 3.79 (t, 8H, *J* = 7.6 Hz, CH_3CH_2*CH_2*OAr), 1.95 (ψ-sext, 8H, CH_3*CH_2*CH_2OAr), 0.99 (t, 12H, *J* = 7.4 Hz, *CH_3*CH_2CH_2O). ^{13}C NMR (100 MHz, $CDCl_3$, 298 K, ppm): δ 156.19, 134.73, 131.12, 130.48, 129.15, 128.92, 126.25, 51.32, 49.61, 30.49, 23.61, 10.16. IR (KBr, ν / cm^{-1}): 3413 (N–H), 1652 (Ar–H), 1467 (C–N), 705(C–H). ESI-MS m/z: $[M + CH_3OH + H]^+$, calcd for $C_{73}H_{93}N_4O_5Cl_4^+$, 1248.36; found, 1249.48. Elemental analyses calcd (%) for

$C_{73}H_{93}N_4O_5Cl_3^+$, 1105.92; found, 1105.43. Calc. for $C_{72}H_{96}Cl_4N_4O_8 \cdot 4H_2O$: C, 67.17; H, 7.52; N, 4.35. Found: C, 66.97; H, 7.55; N, 4.27.

5,11,17,23-Tetra-(*N*-phenylethyl-*N*-methyleneamine)-25,26,27,28-tetrapropoxy-calix[4]arene (calix-phenylethyl-amine)

A method as described previously for 5,11,17,23-tetra-(*N*-phenylmethyl-*N*-methyleneamine)-25,26,27,28-tetrapropoxycalix[4]arene was employed to produce the target compound (Yield: 270 mg, 75 %) as a white solid. mp. 235–237 ºC. ^{1}H NMR (400 MHz, DMSO-d_6, 298 K): δ = 9.43 (s, 8H, HCl·HN=C), 7.23 (m, 24H, *Ar*–CH_2N), 4.38 (d, 4H, *J* = 12.8 Hz, Ar–*CH_2*–Ar), 3.97 (s, 8H, *J* = 12.2 Hz, Ar–CH_2–N), 3.84 (s, 8H, CH_3CH_2*CH_2*OAr), 3.23 (t, 4H, *J* = 12.8 Hz, Ar–*CH_2*–Ar), 3.11 (s, 16H, Ar–*CH_2*–N), 1.90 (ψ-sext, 8H, CH_3*CH_2*CH_2OAr), 0.99 (t, 12H, *J* = 7.4 Hz, *CH_3*CH_2CH_2OAr). ^{13}C NMR (100 MHz, $CDCl_3$, 298 K, ppm): δ 156.35, 136.77, 134.81, 131.78, 128.70, 128.56, 126.68, 126.05, 51.07, 49.90, 32.14, 30.60, 23.20, 10.20. IR (KBr, ν / cm^{-1}): 3423 (N–H), 1616 (Ar–H), 1456 (C–N), 752 (C–H). ESI-MS m/z: $[M+H]^+$, calcd for $C_{76}H_{97}N_4O_4Cl_4^+$, 1269.63; found, 1270.31, $[M+CH_3OH+H]^+$, calcd for $C_{77}H_{101}N_4O_5Cl_4^+$, 1304.46; found, 1304.38. Elemental analyses calcd (%) for $C_{76}H_{100}Cl_4N_4O_6 \cdot 2H_2O$: C, 69.82; H, 7.71; N, 4.29. Found: C, 69.85; H, 7.65; N, 4.28.

5,11,17,23-Tetra-(*N*-thienylmethyl-*N*-methyleneamine)-25,26,27,28-tetra-propoxycalix[4]arene (calix-thienylmethyl-amine)

A method as described previously for 5,11,17,23-tetra-(*N*-phenylmethyl-*N*-methyleneamine)-25,26,27,28-tetrapropoxycalix[4]arene was employed to produce the target compund (Yield: 230 mg, 85 %) as a white solid. mp. 235–237 ºC. ^{1}H NMR (400 MHz, DMSO-d_6, 298 K): δ = 9.87 (s, 8H, HCl·HN=C), 7.61 (d, 8H, *J* = 8.4 Hz, thienyl-H), 7.27 (d, 8H, *J* = 8.4 Hz, thienyl-H), 7.04 (d, 8H, *J* = 8.4 Hz, thienyl-H), 7.05 (s, 8H, Ar–H), 4.38, 3.23 (d, 4H, *J* = 12.8 Hz, Ar–CH_2–Ar), 4.24 (s, 8H, thienyl–CH_2–N), 3.81 (s, 8H, $CH_3CH_2CH_2$OAr), 3.47 (s, 8H, Ar–CH_2–N), 1.95 (ψ-sext, 8H, $CH_3CH_2CH_2$OAr), 1.08 (t, 12H, *J* = 7.4 Hz, $CH_3CH_2CH_2$O). ^{13}C NMR (100 MHz, $CDCl_3$, 298 K, ppm): δ 207.1, 156.22, 134.81, 131.81, 131.26, 127.93, 127.55, 126.10, 49.16, 45.15, 30.93, 30.44, 23.17, 10.15. IR (KBr, ν / cm^{-1}): 3394 (N–H), 1633 (Ar–H), 1467 (C–N), 752 (C–H). ESI-MS m/z: $[M+K^+]^+$, calcd for $C_{64}H_{81}N_4O_4S_4Cl_4K^+$, 1276.35; found, 1276.39. Elemental analyses calcd (%) for $C_{66}H_{84}Cl_8N_4O_4S_4$•$2CH_2Cl_2$: C, 56.25; H, 6.01; N, 3.98. Found: C, 56.53; H, 6.02; N, 4.01.

The general synthesis of tetra-(dithiocarbamato)-25,26,27,28-tetrapropoxy-calix[4]arene ligands K_4L^n (n = 1–3).

KOH (1 mmol) and CS_2 (1 mmol) were added to a solution of respective tetra-amino calix[4]arene (0.25 mmol) in CH_3OH (2 mL). The mixture was stirred at room temperature for 4 h, after which a yellow precipitate started to form. The yellow solid was filtered off, washed with diethyl ether (10 mL) and dried under vacuum. The light yellow products were used for further experiments without any purification.

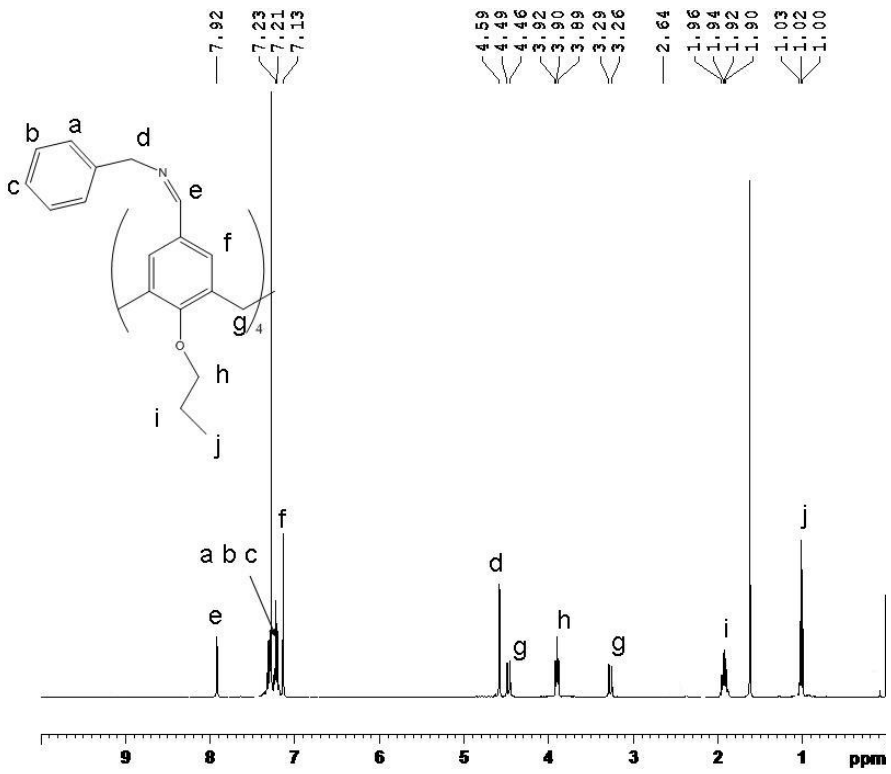

Figure S1. ^{1}H NMR spectrum of calix-phenylmethyl-imine in $CDCl_3$ at 298 K.

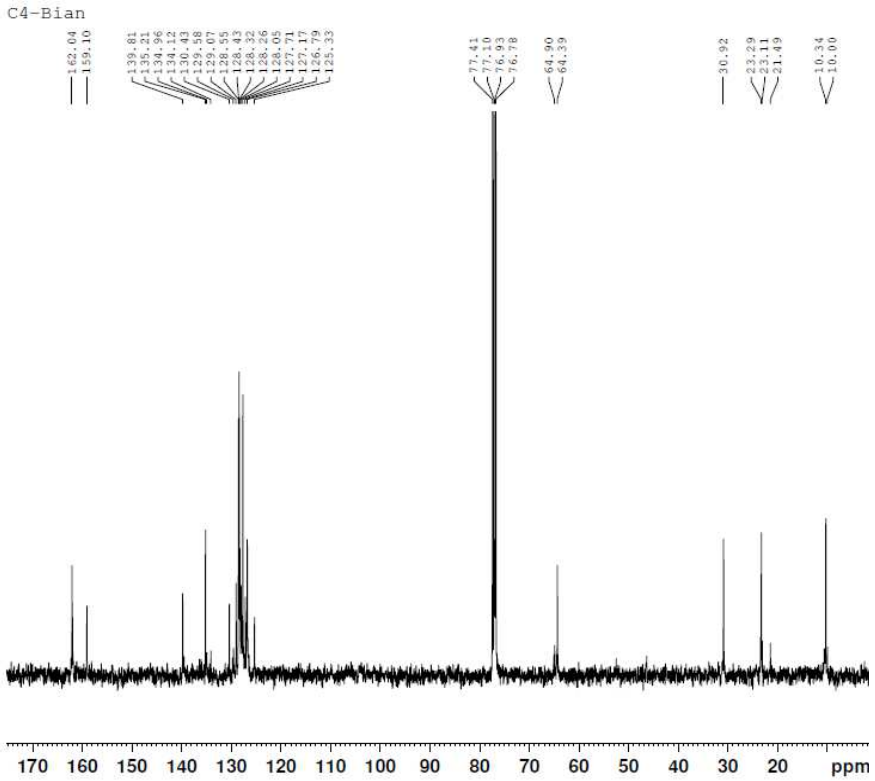

Figure S2. ^{13}C NMR spectrum of calix-phenylmethyl-imine in $CDCl_3$ at 298 K.

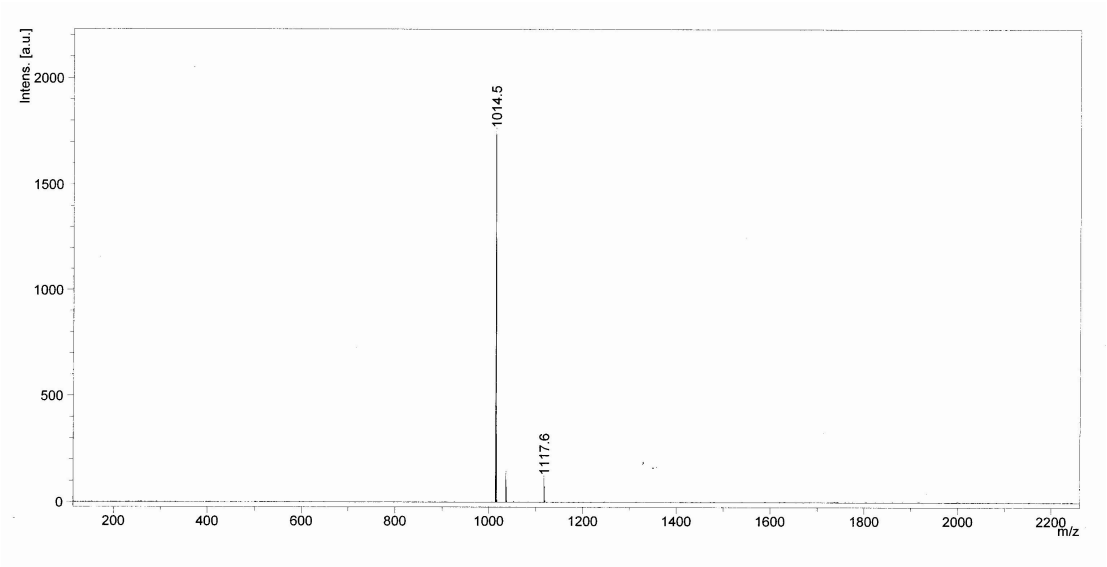

Figure S3. MALDI-TOF-MS spectrum of calix-phenylmethyl-imine in CH_3OH.

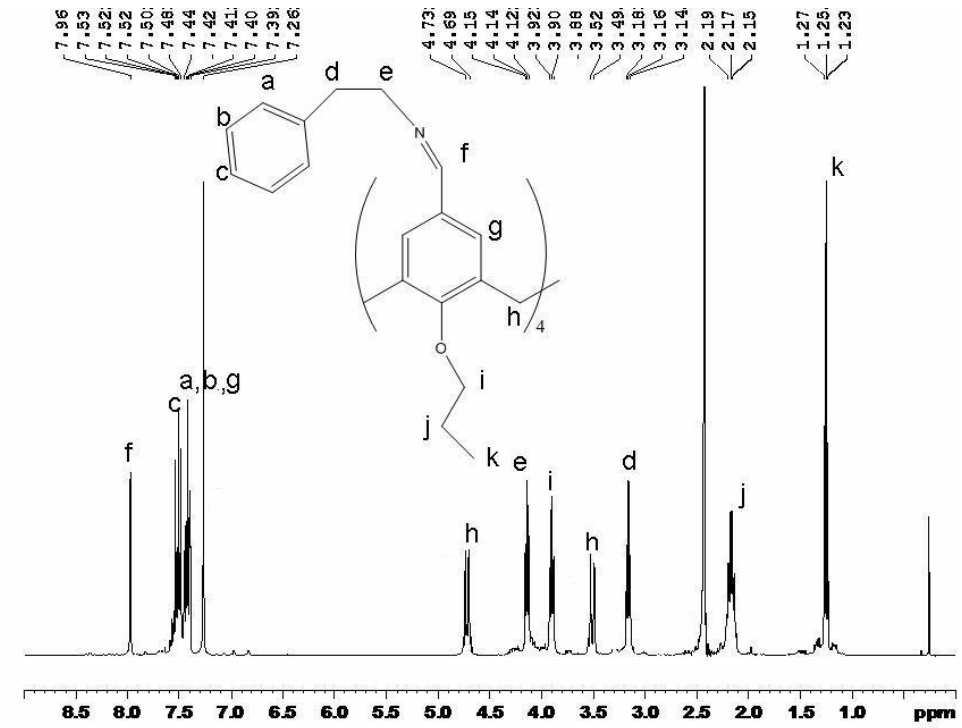

Figure S4. ^1H NMR spectrum of calix-phenylethyl-imine in $CDCl_3$ at 298 K.

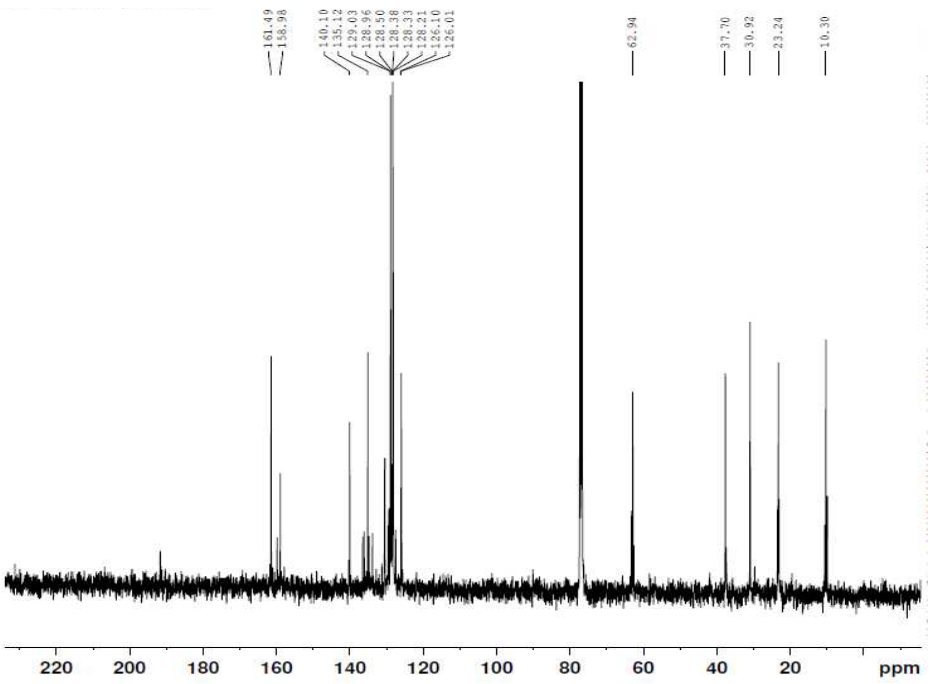

Figure S5. ^{13}C NMR spectrum of calix-phenylethyl-imine in $CDCl_3$ at 298 K.

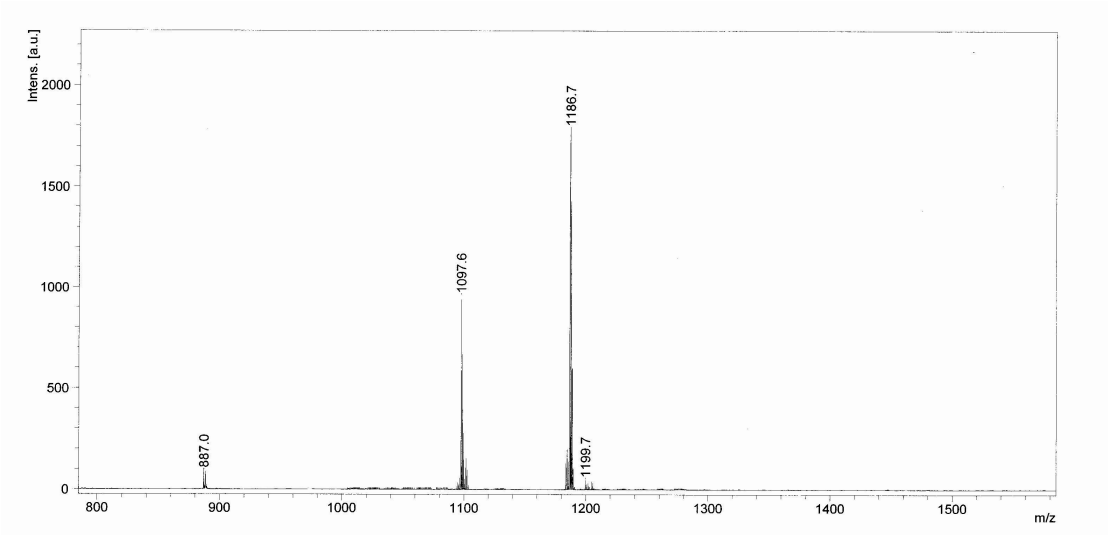

Figure S6. MALDI-TOF-MS spectrum of calix-phenylethyl-imine in CH_3OH.

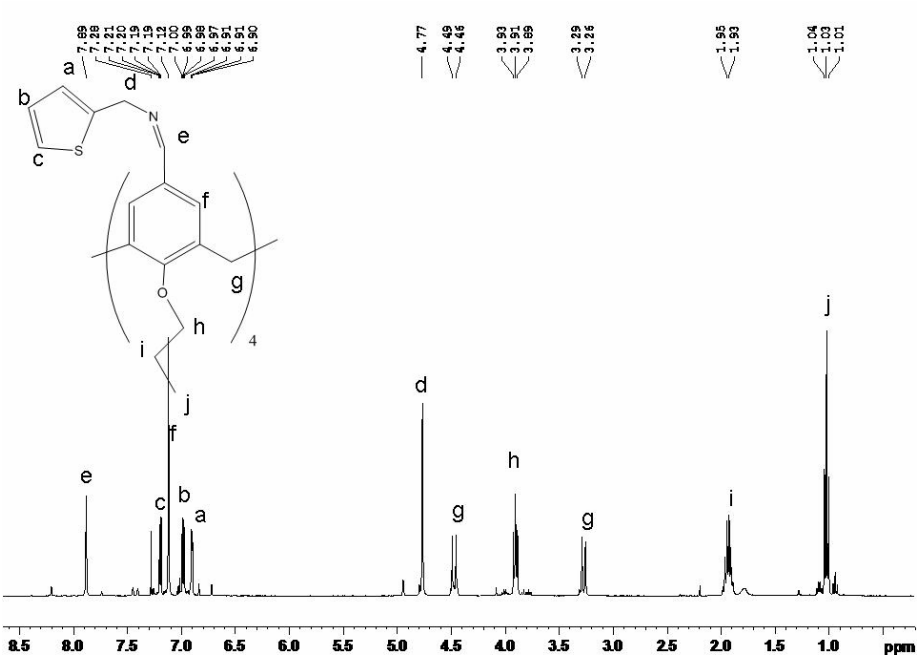

Figure S7. ^{1}H NMR spectrum of calix-thienylmethyl-imine in DMSO-d_6 at 298 K.

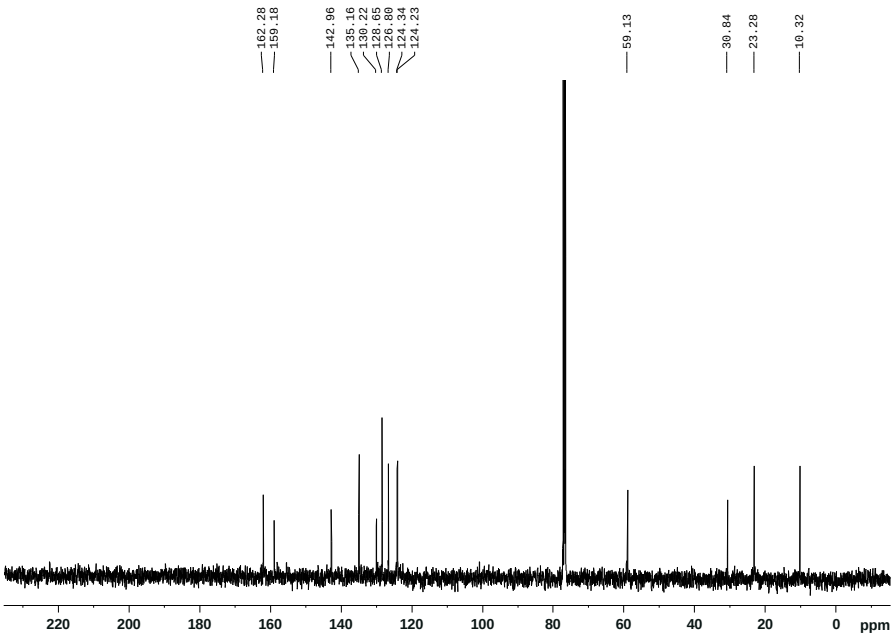

Figure S8. ^{13}C NMR spectrum of calix-thienylmethyl-imine in $CDCl_3$ at 298 K.

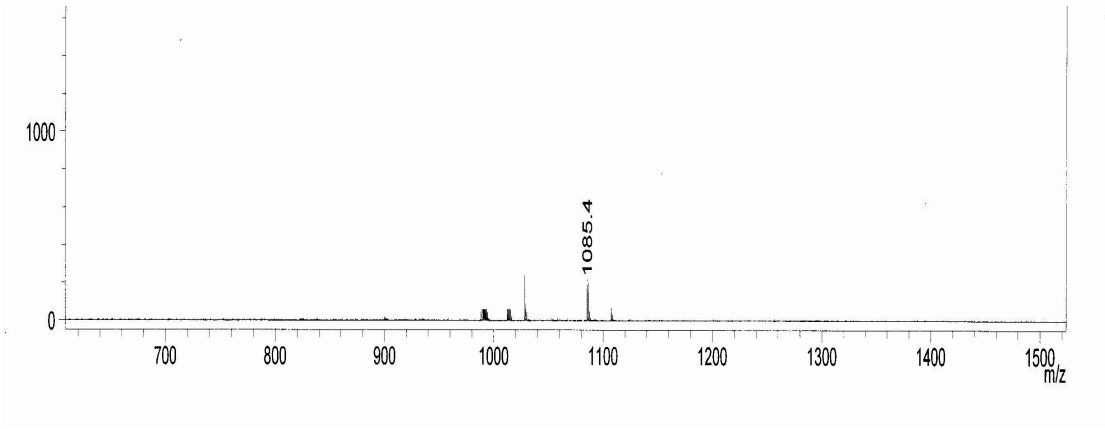

Figure S9. MALDI-TOF-MS spectrum of calix-thienylmethyl-imine in CH_3OH.

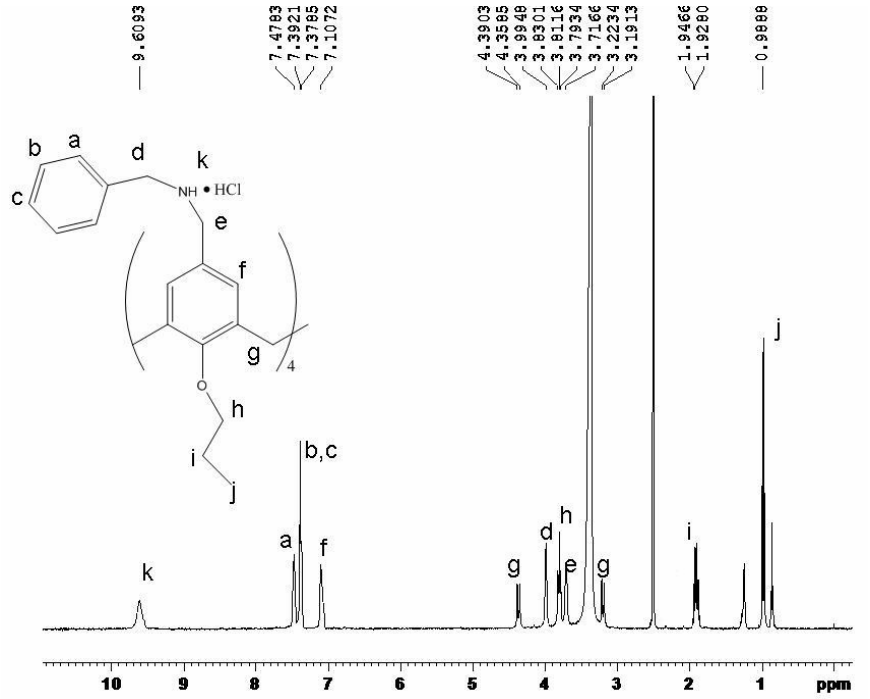

Figure S10. ^{1}H NMR spectrum of calix-phenylmethyl-amine in DMSO-d_6 at 298 K.

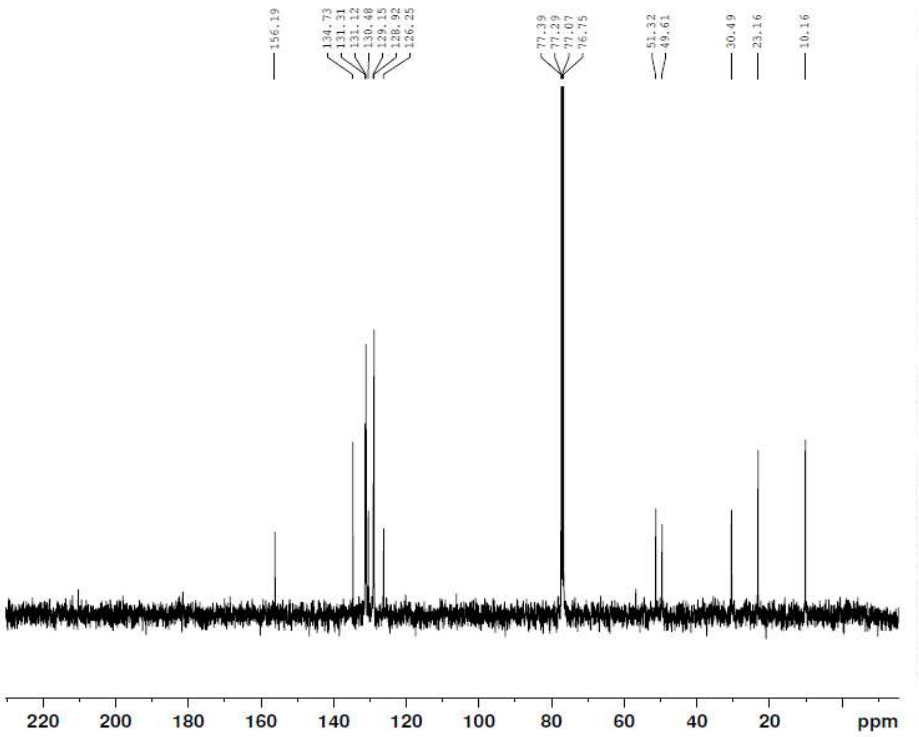

Figure S11. ^{13}C NMR spectrum of calix-phenylmethyl-amine in DMSO-d_6 at 298 K.

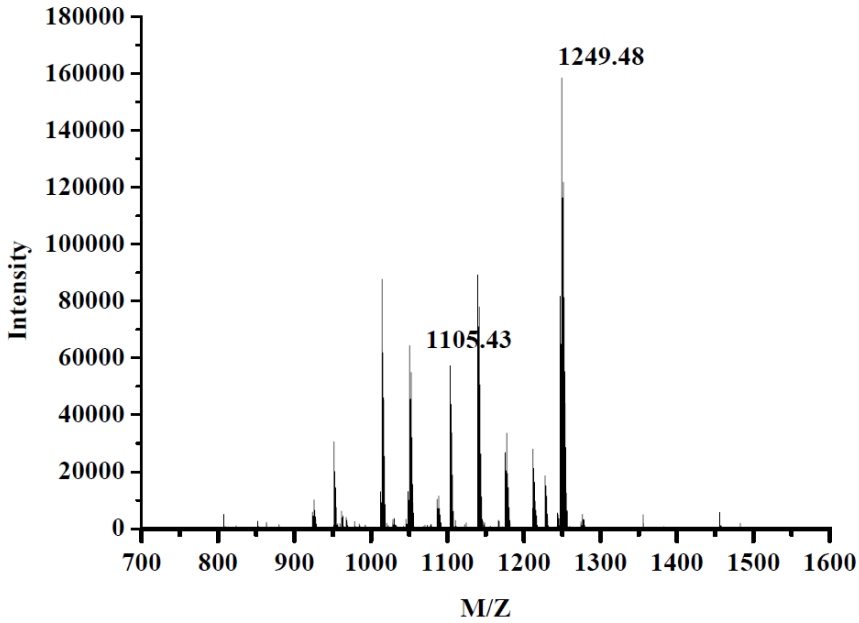

Figure S12. ESI-MS spectrum of calix-phenylmethyl-amine in CH_3OH at 298 K.

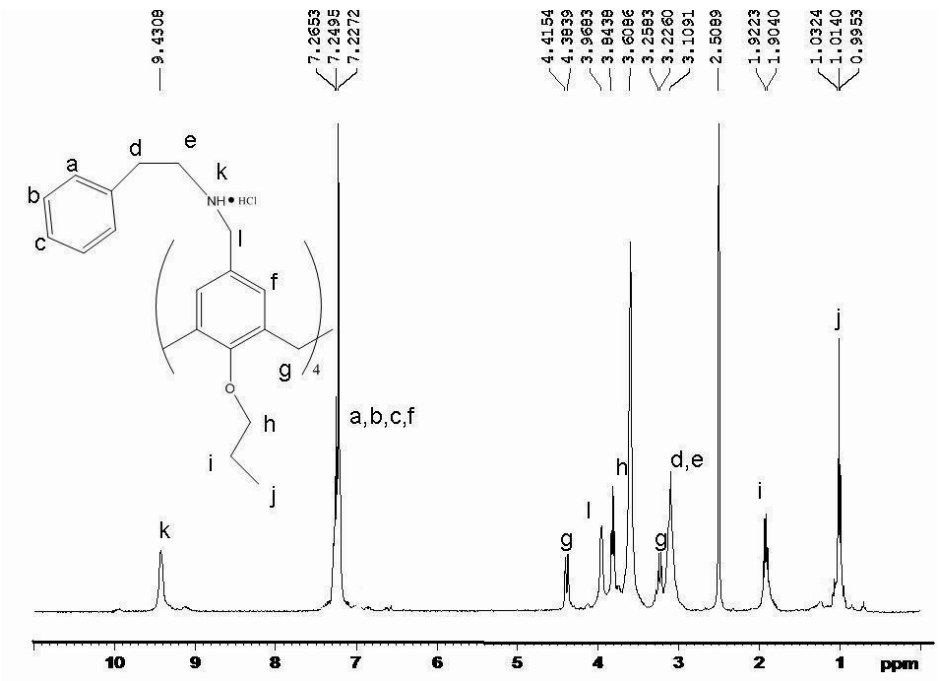

Figure S13. ^{1}H NMR spectrum of calix-phenylethyl-amine in DMSO-d_6 at 298 K.

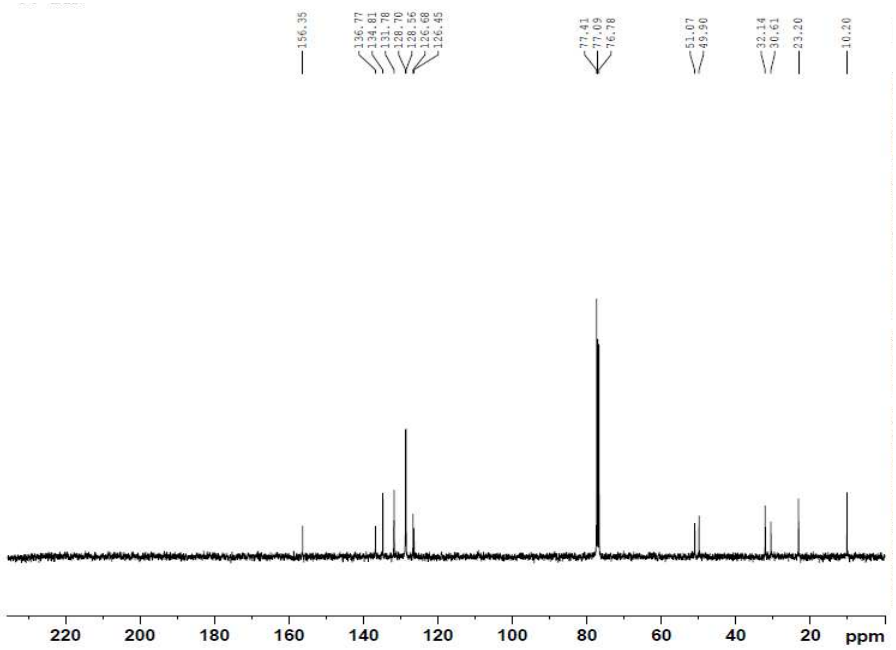

Figure S14. ^{13}C NMR spectrum of calix-phenylethyl-amine in DMSO-d_6 at 298 K.

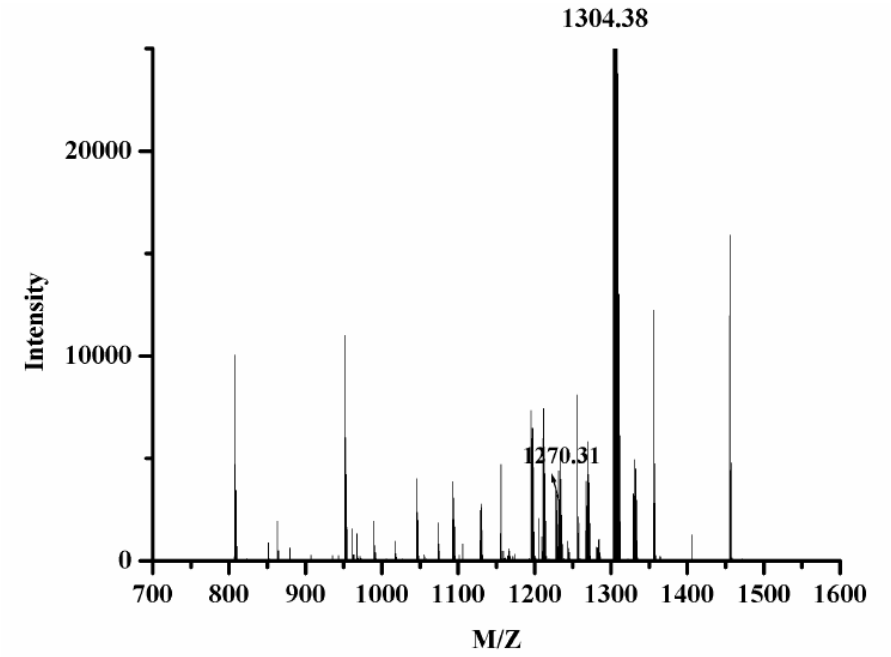

Figure S15. ESI-MS spectrum of calix-phenylethyl-amine in CH_3OH at 298 K.

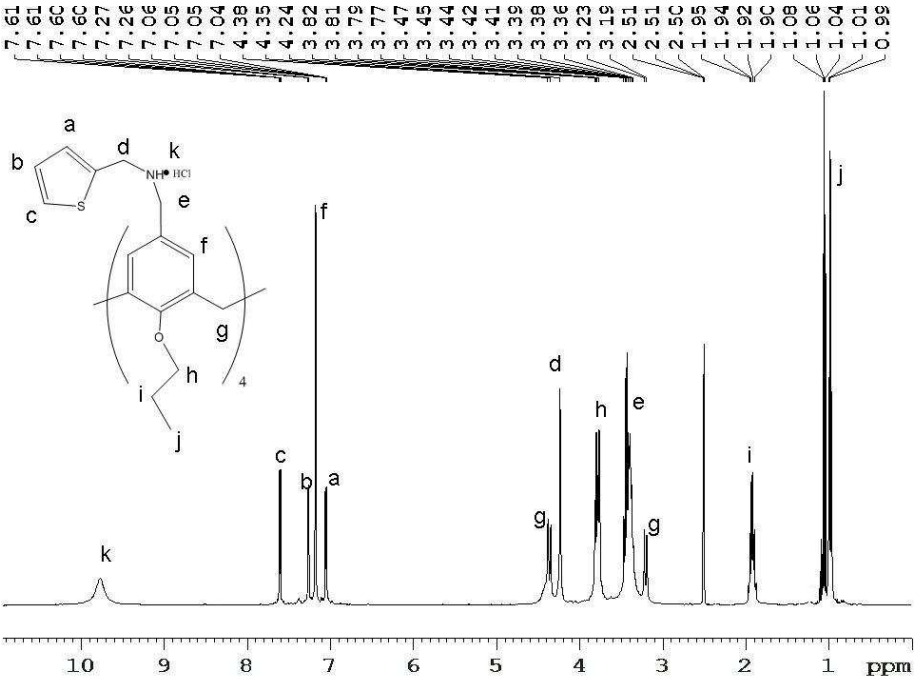

Figure S16. ^{1}H NMR spectrum of calix-thienylmethyl-amine in DMSO-d_6 at 298 K.

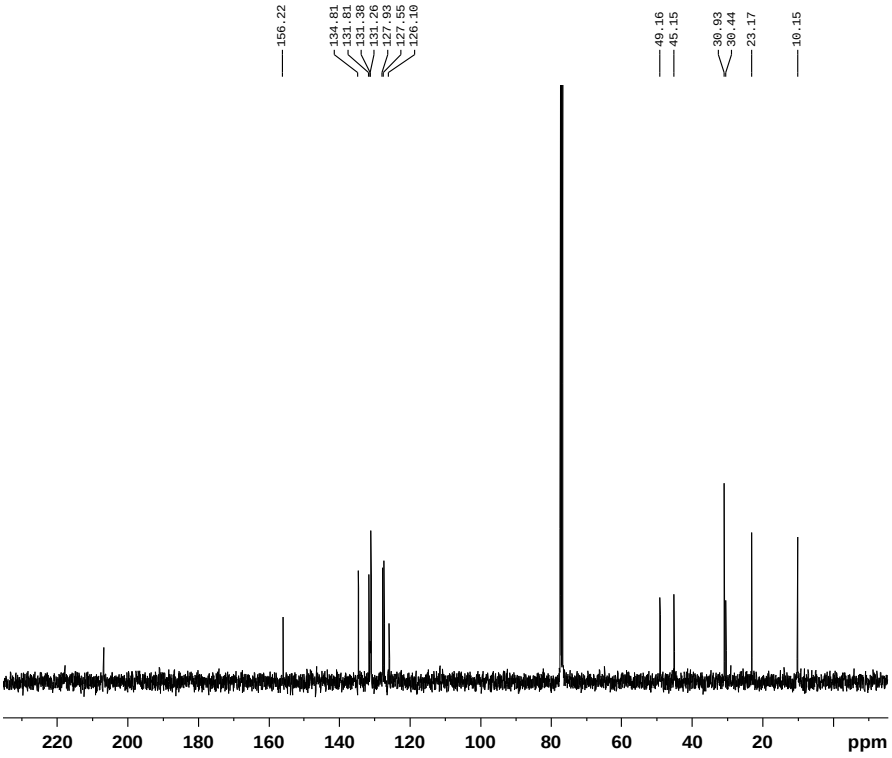

Figure S17. ^{13}C NMR spectrum of calix-thienylmethyl-amine in DMSO-d_6 at 298 K.

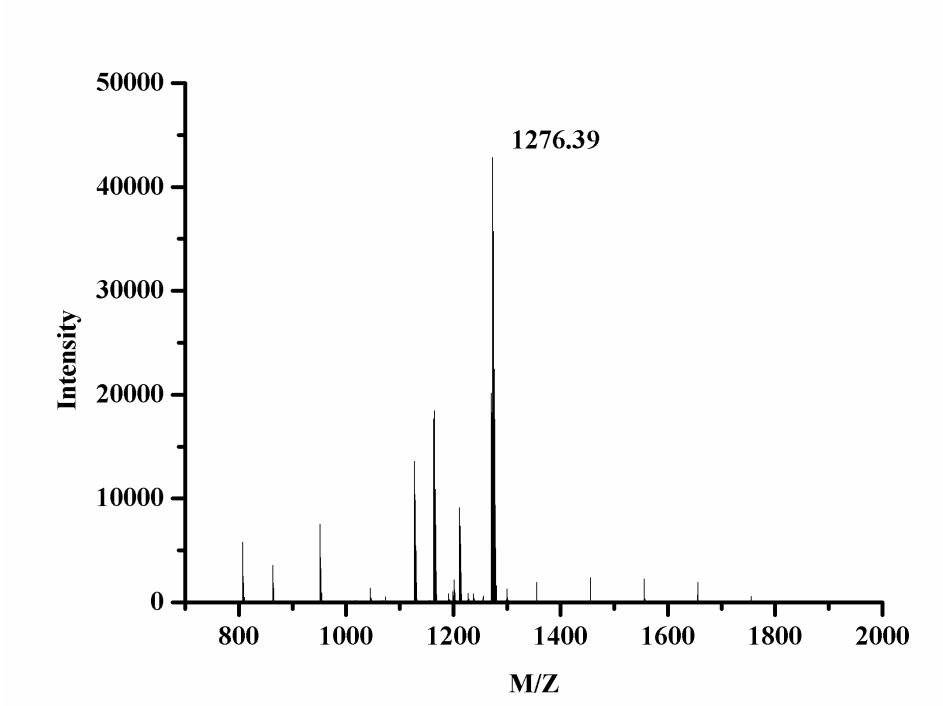

Figure S18. ESI-MS spectrum of calix-thienylmethyl-amine in CH_3OH at 298 K.

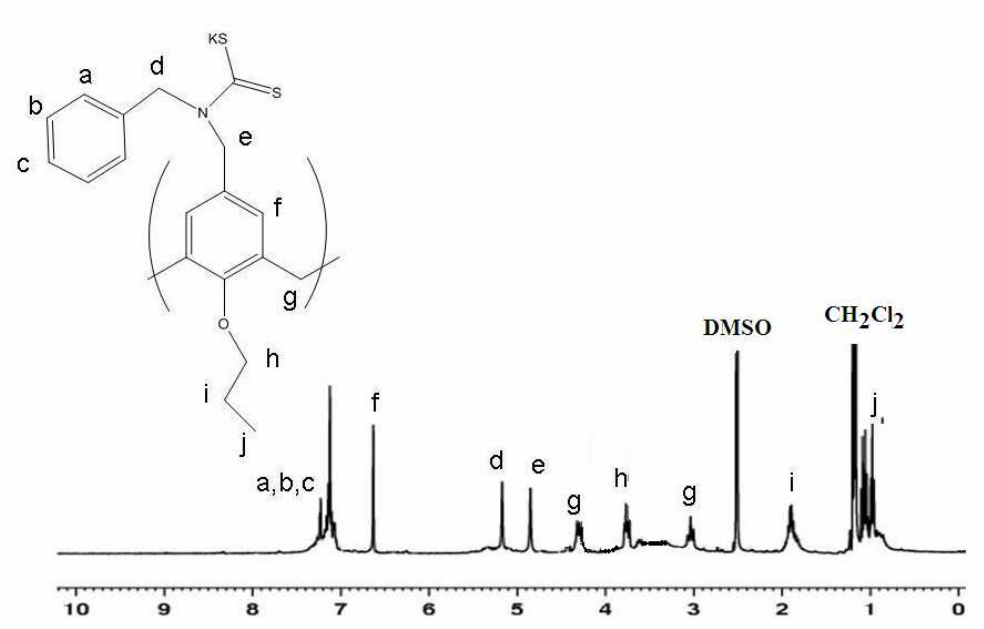

Figure S19. ^{1}H NMR spectrum of K_4L^1 in DMSO-d_6 at 298 K.

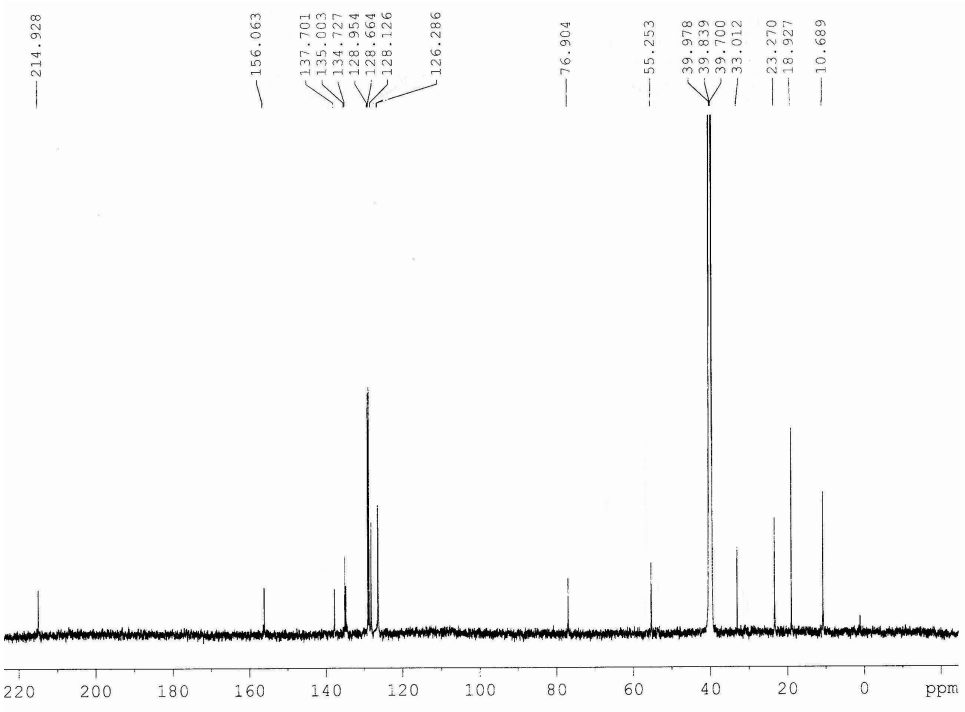

Figure S20. ^{13}C NMR spectrum of K_4L^1 in DMSO-d_6 at 298 K.

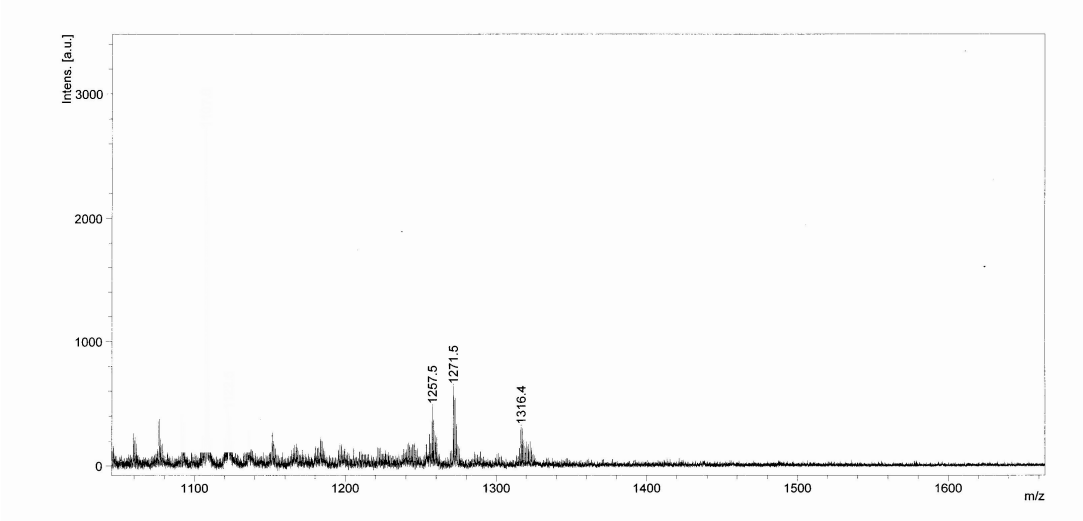

Figure S21. MALDI-TOF-MS spectrum of K_4L^1 in CH_3OH.

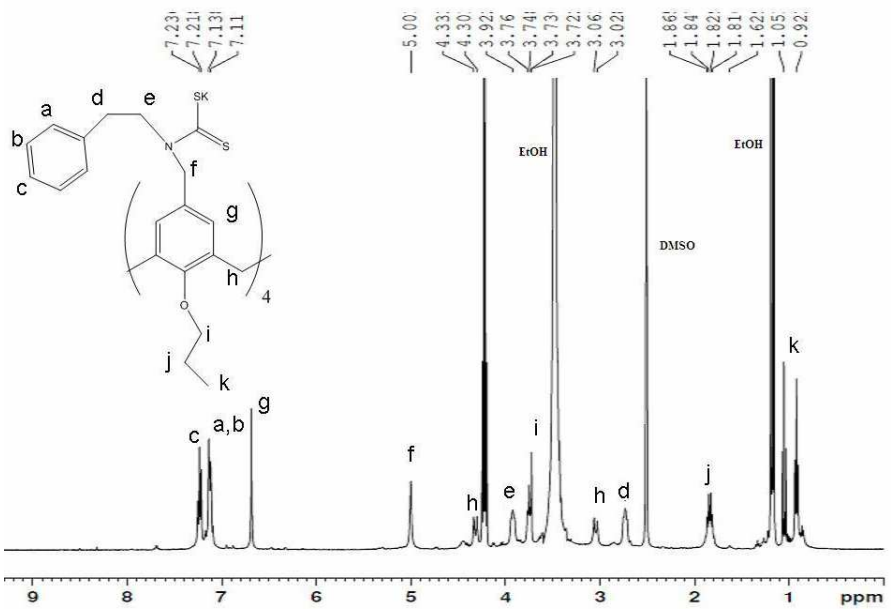

Figure S22. ^{1}H NMR spectrum of K_4L^2 in DMSO-d_6 at 298 K.

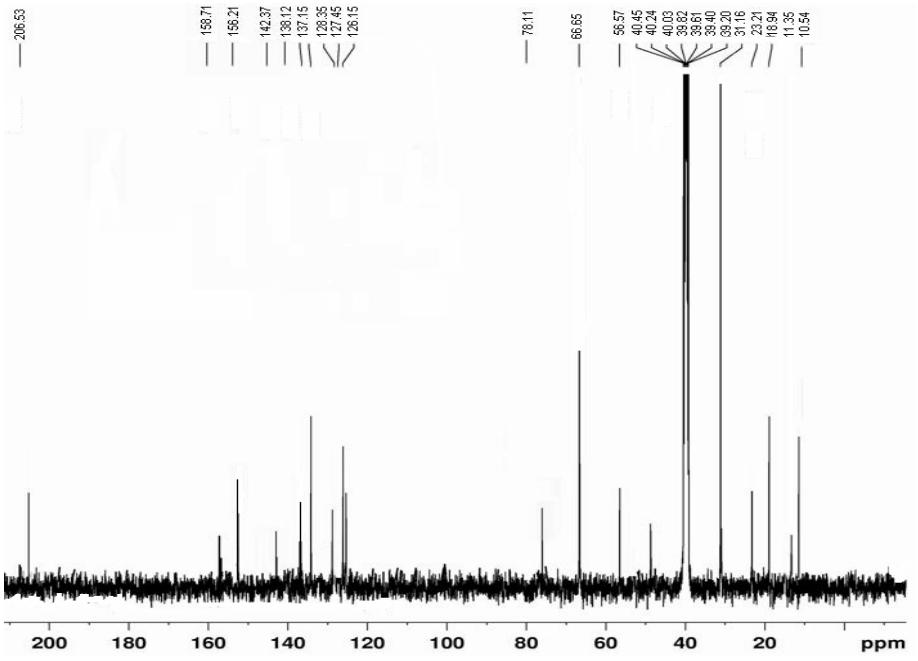

Figure S23. ^{13}C NMR spectrum of K_4L^2 in DMSO-d_6 at 298 K.

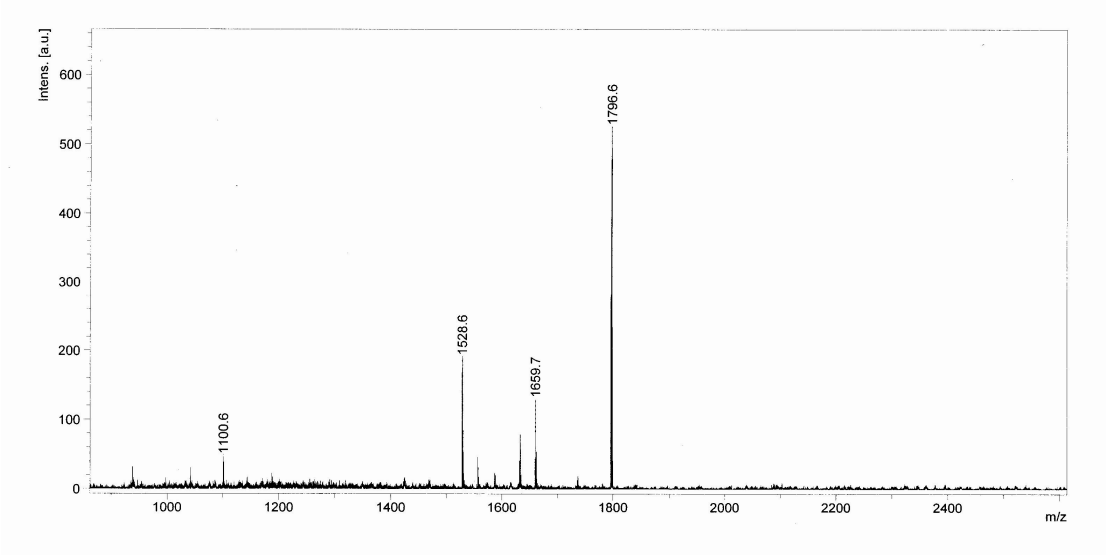

Figure S24. MALDI-TOF-MS spectrum of K_4L^2 in CH_3OH.

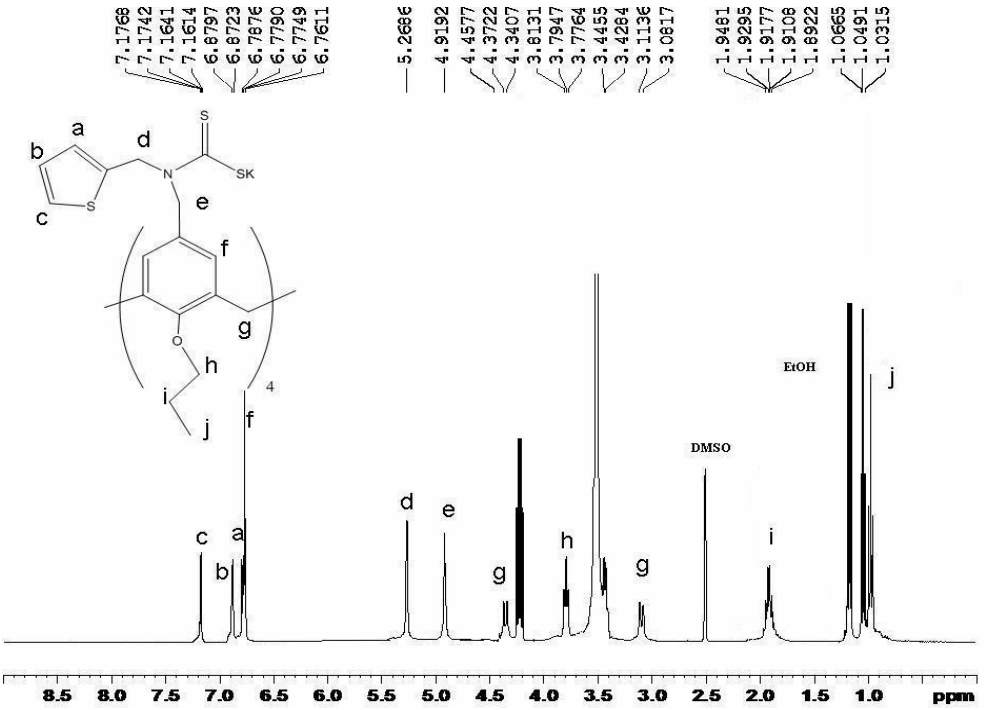

Figure S25. ^{1}H NMR spectrum of K_4L^3 in DMSO-d_6 at 298 K.

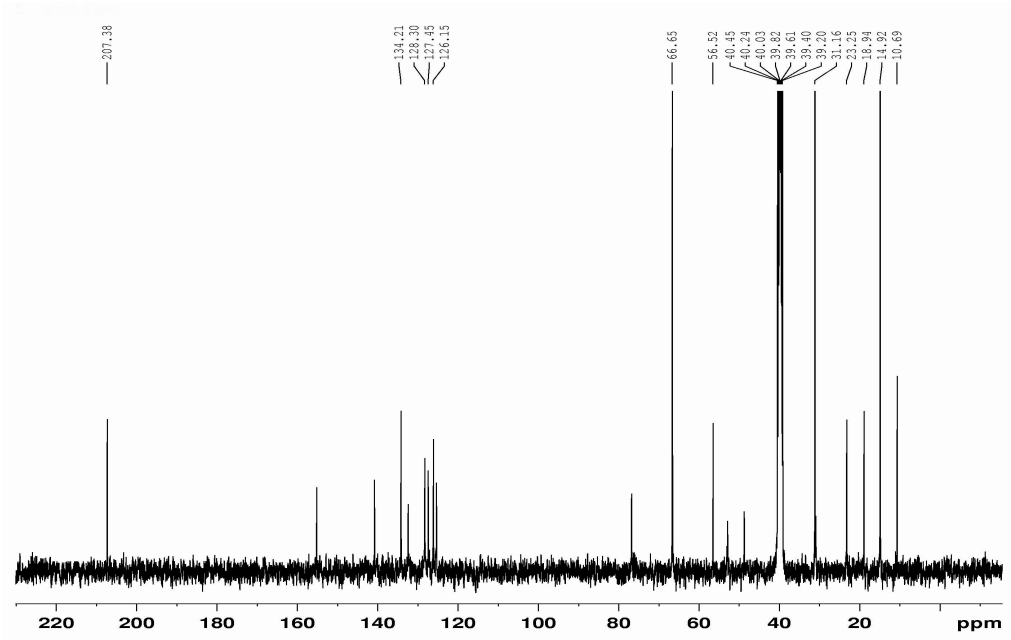

Figure S26. ^{1}H NMR spectrum of K_4L^3 in DMSO-d_6 at 298 K.

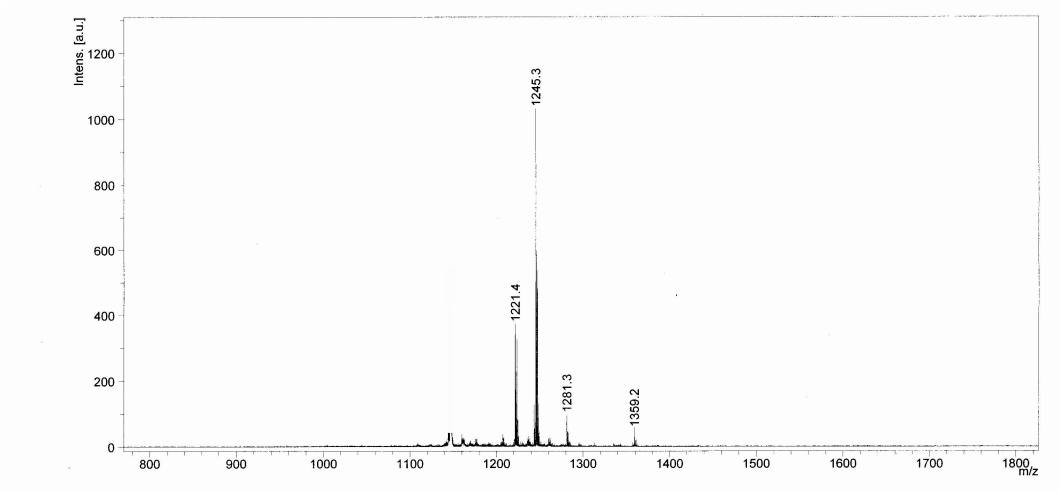

Figure S27. MALDI-TOF-MS spectrum of K_4L^3 in CH_3OH.

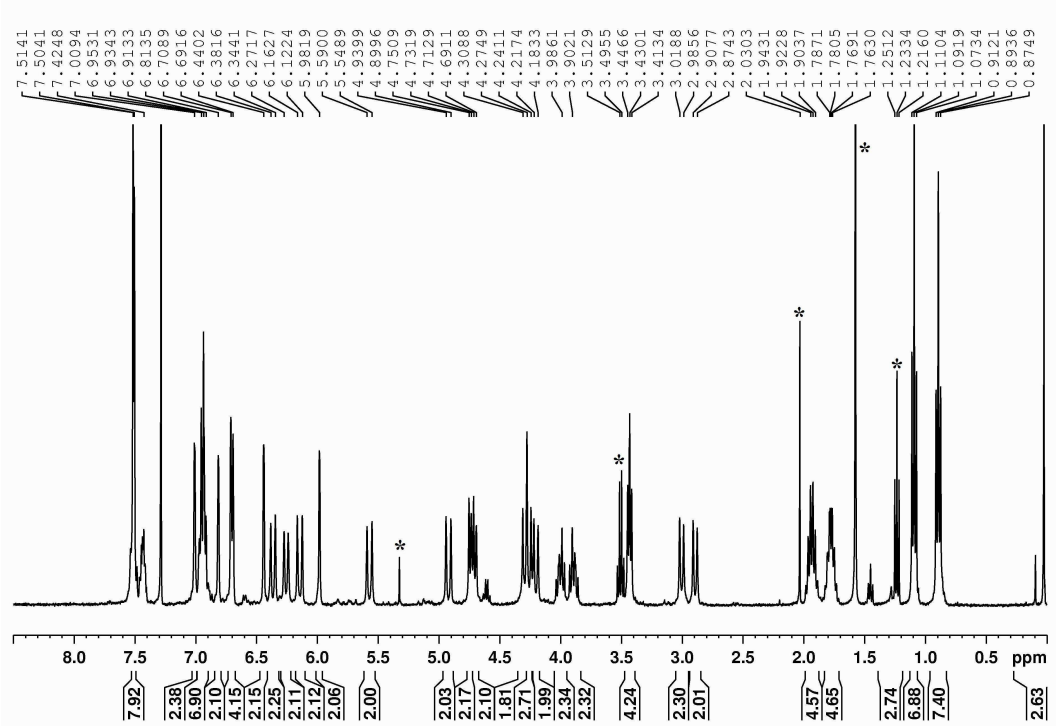

Figure S28. ^1H NMR spectrum of complex **1** in $CDCl_3$ at 298 K (The signals of solvents were labeled with ∗).

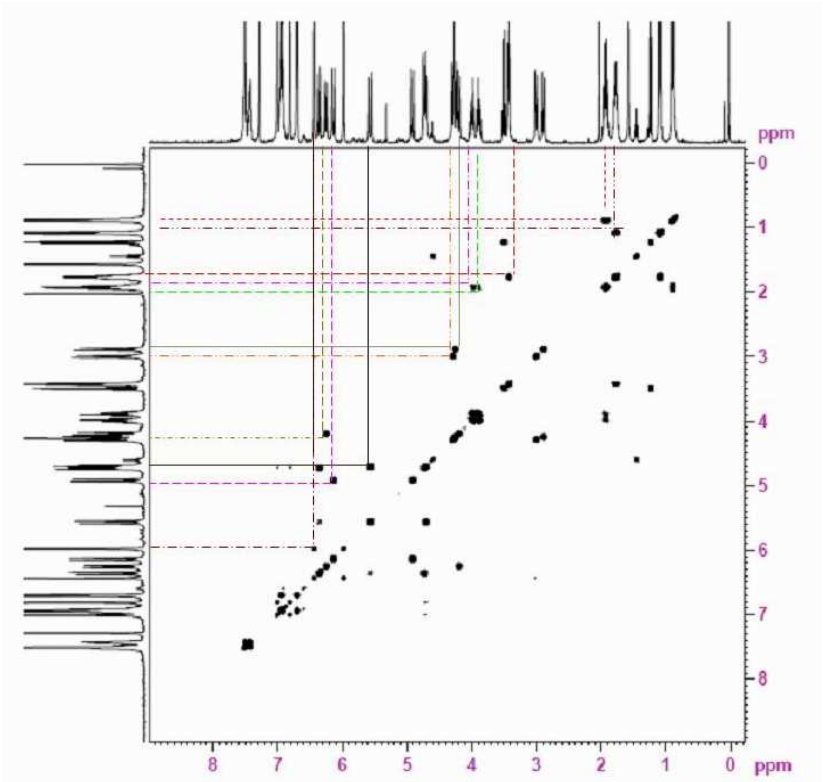

Figure S29. ^{1}H-^{1}H COSY NMR spectrum of complex **1** in $CDCl_3$ at 298 K.

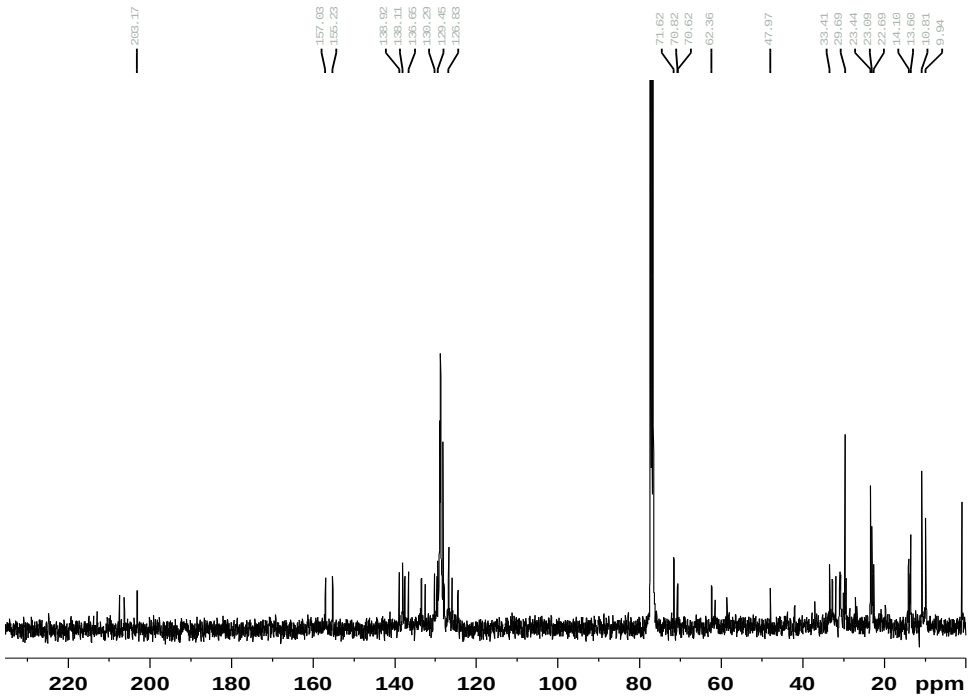

Figure S30. ^{13}C NMR spectrum of complex **1** in $CDCl_3$ at 298 K.

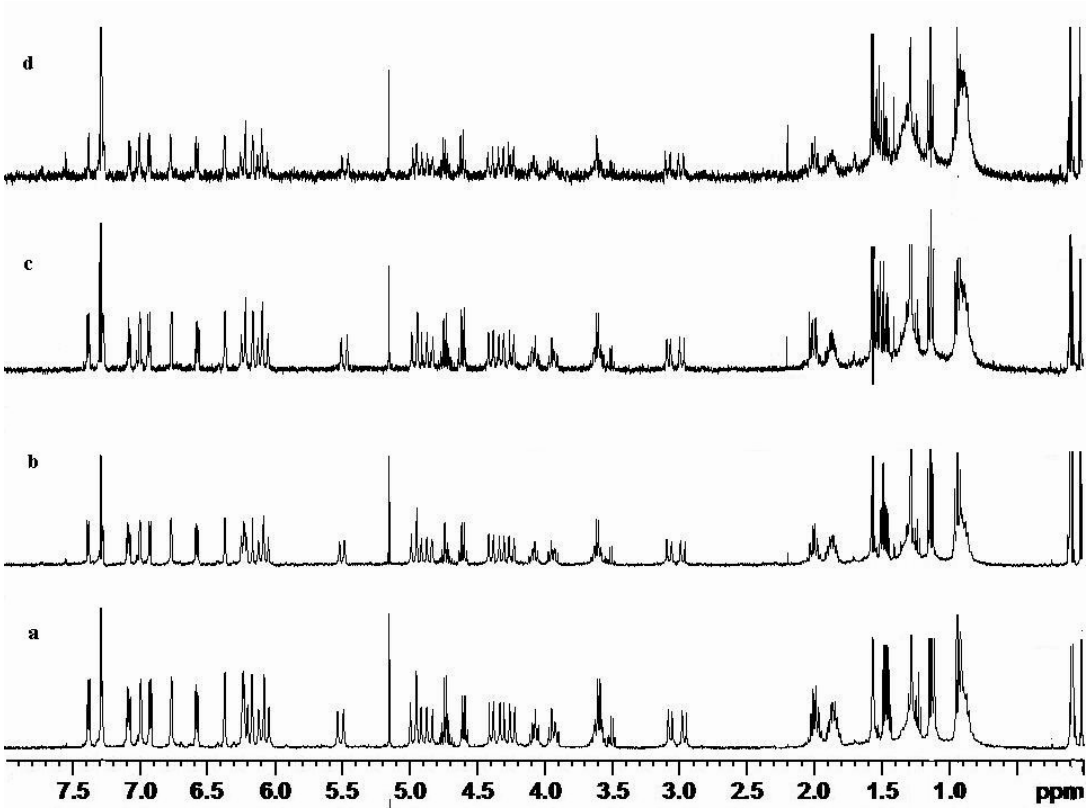

Figure S31. ^{1}H NMR spectra of complex **1** at different concentrations in $CDCl_3$ (a, 4.17 mM; b, 2.15 mM; c, 1.21 mM; d, 0.42 mM) at 298 K.

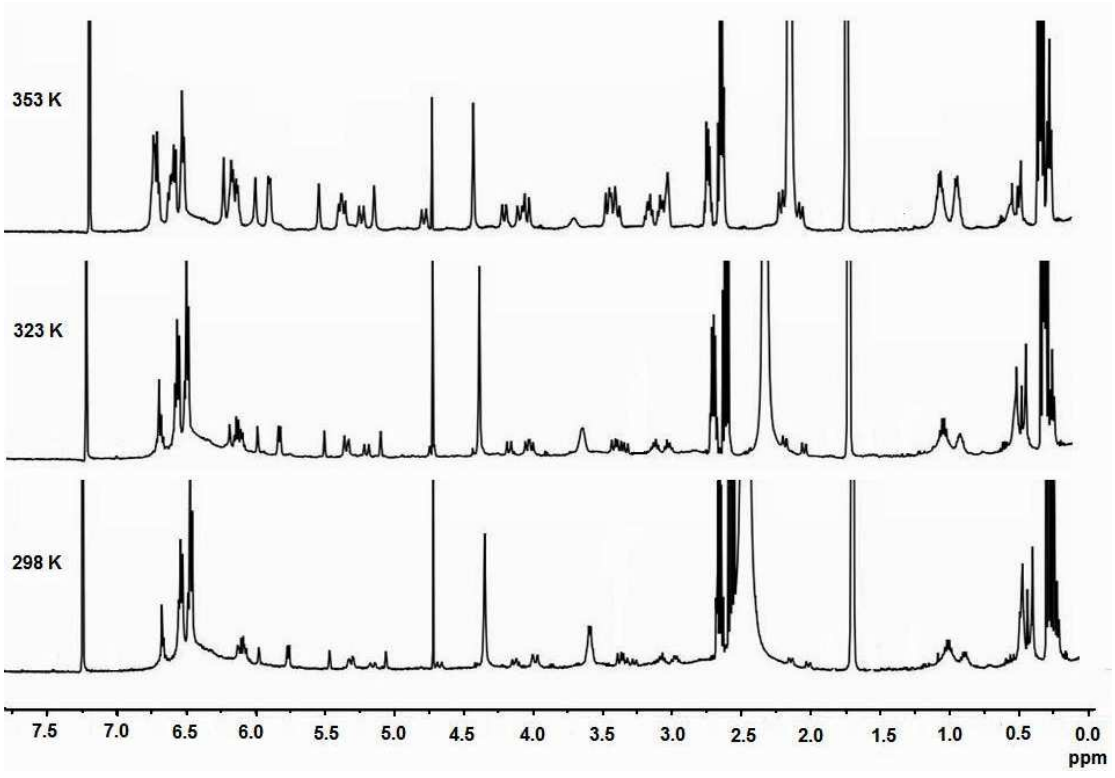

Figure S32. Variable-temperature ^{1}H NMR spectra of complex **1** in $CDCl_3$/d_6-DMSO (1:2, v/v) (Bottom to top: 298 K, 323 K and 353 K) (500 MHz).

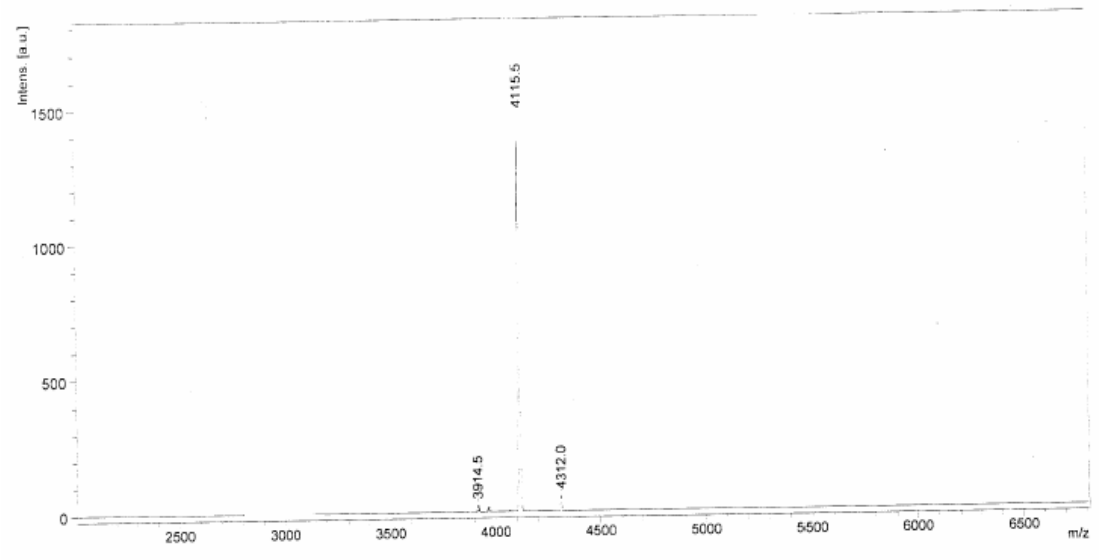

Figure S33. MALDI-TOF-MS spectrum of complex **1** in $CHCl_3$ at 298 K.

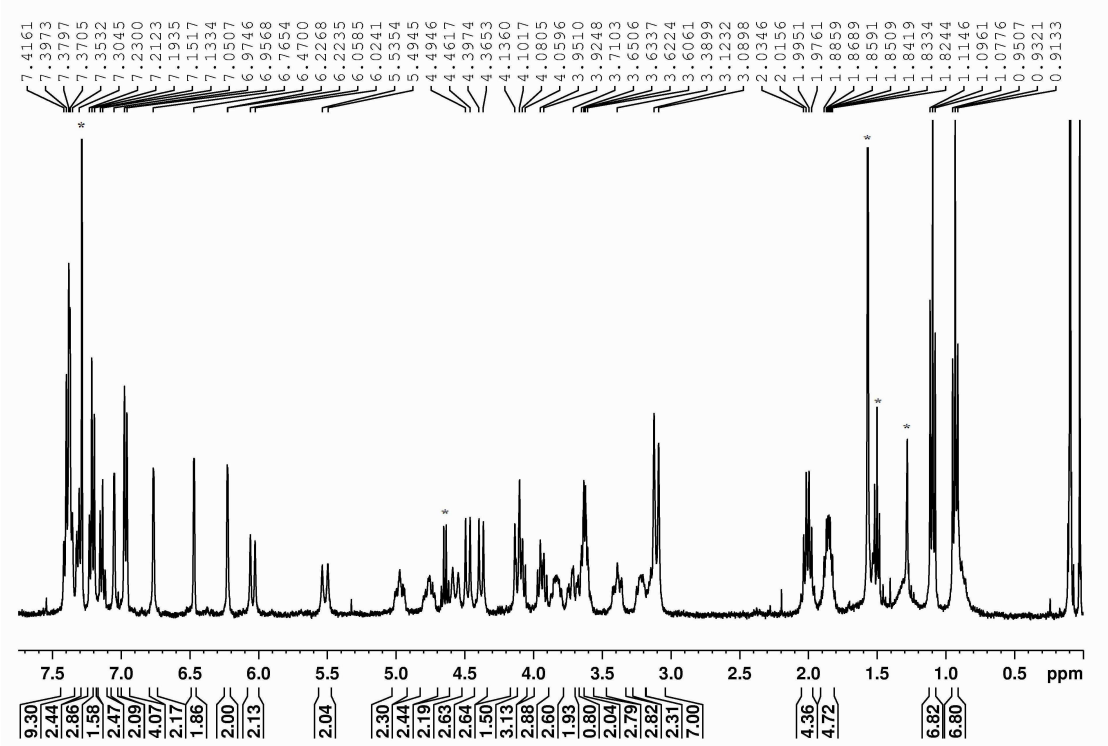

Figure S34. ^1H NMR spectrum of complex **2** in $CDCl_3$ at 298 K (The signals of solvents were labeled with ∗).

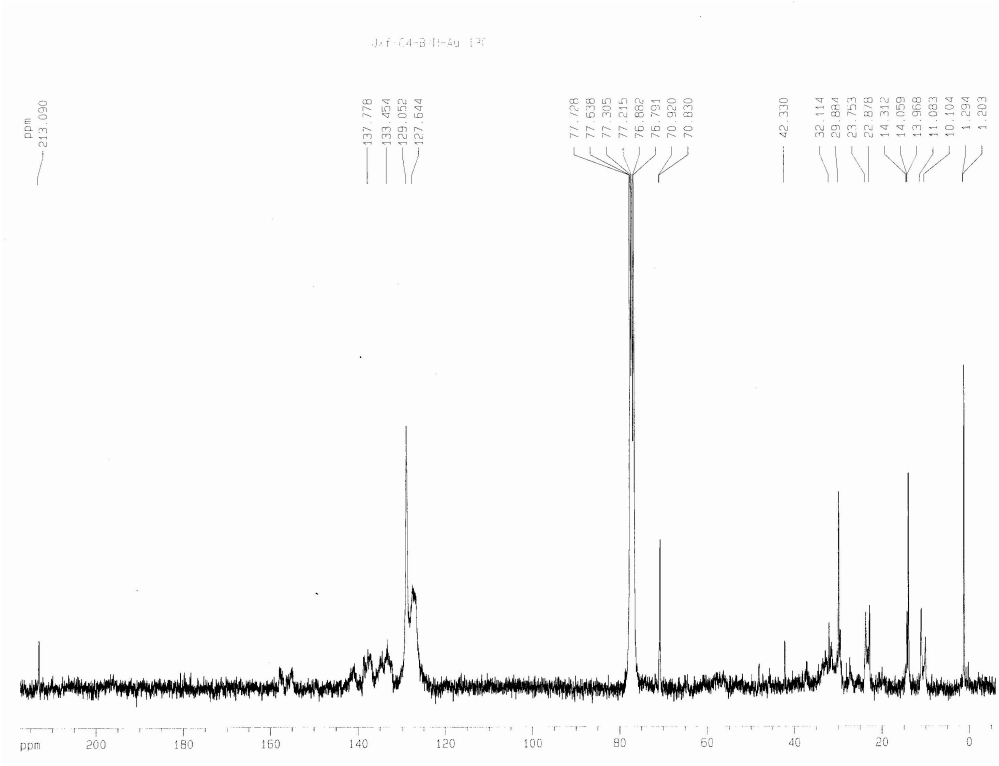

Figure S35. ^{13}C NMR spectrum of complex **2** in $CDCl_3$ at 298 K.

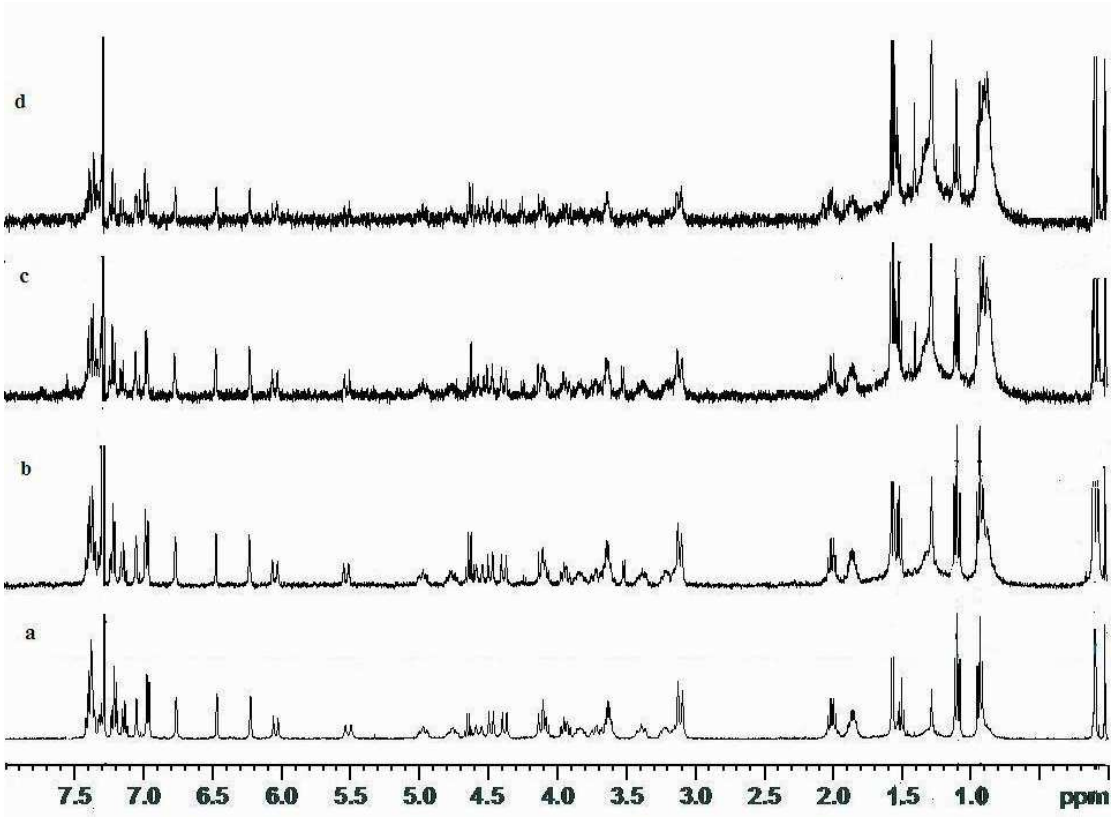

Figure S36. ^{1}H NMR spectra of complex **2** at different concentrations in $CDCl_3$ (a, 2.41 mM; b,1.21 mM; c, 0.63 mM; d, 0.23 mM) at 298 K.

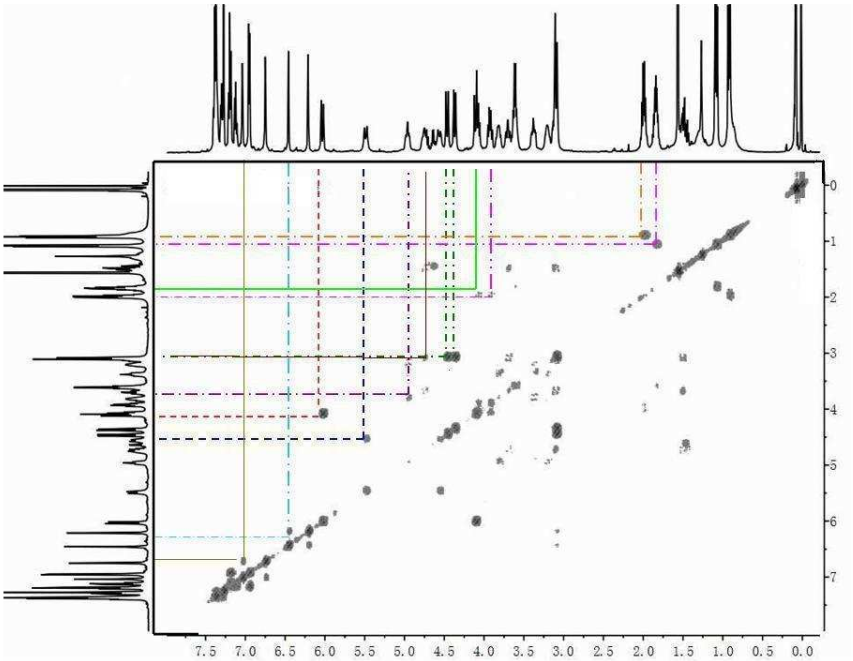

Figure S37. ^{1}H-^{1}H COSY NMR spectrum of complex **2** in $CDCl_3$ at 298 K (500 MHz).

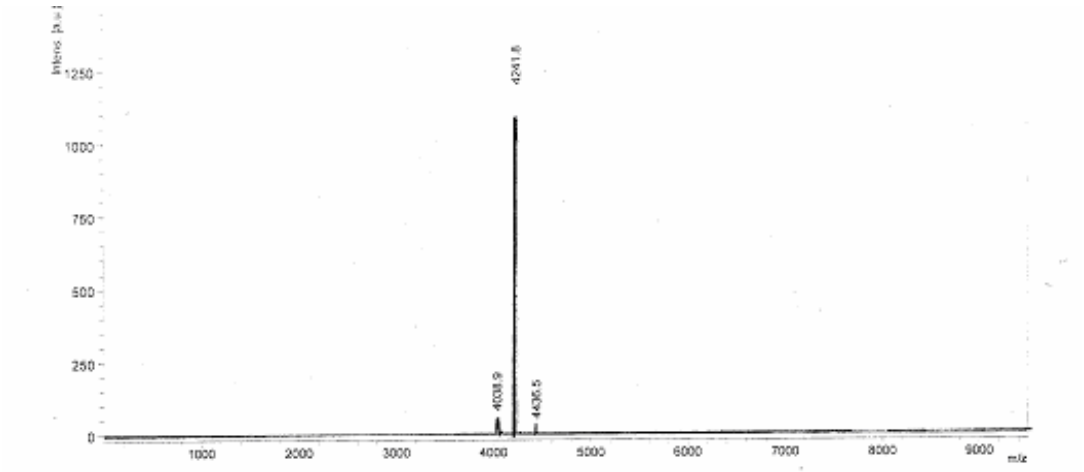

Figure S38. MALDI-TOF-MS spectrum of complex **2** in $CHCl_3$ at 298 K.

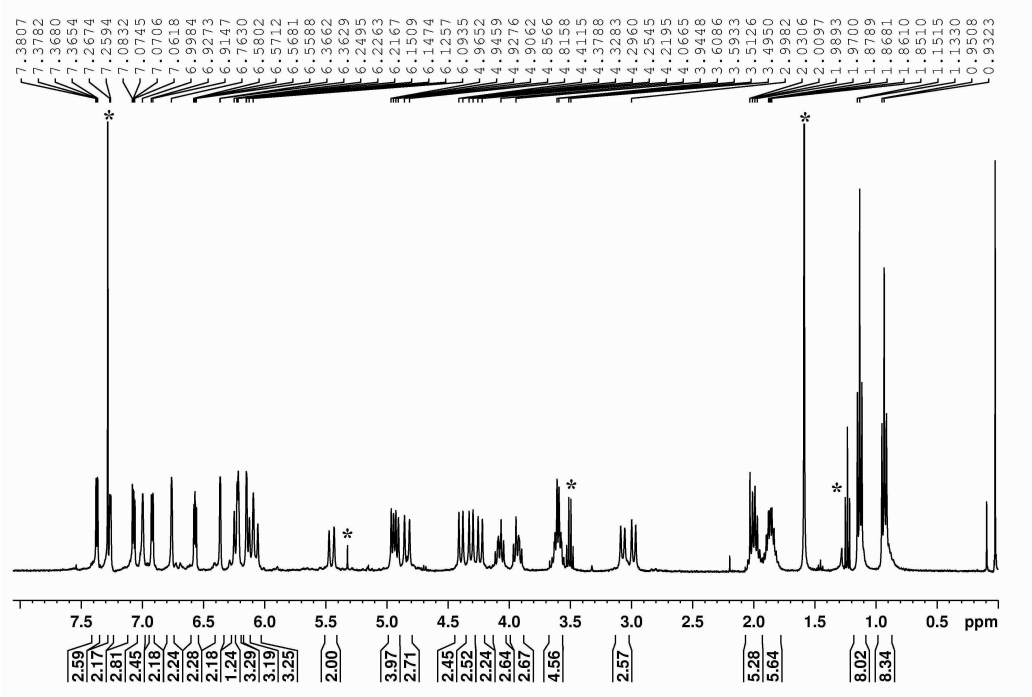

Figure S39. ^{1}H NMR spectrum of complex **3** in $CDCl_3$ at 298 K (The signals of solvents were labeled with ∗).

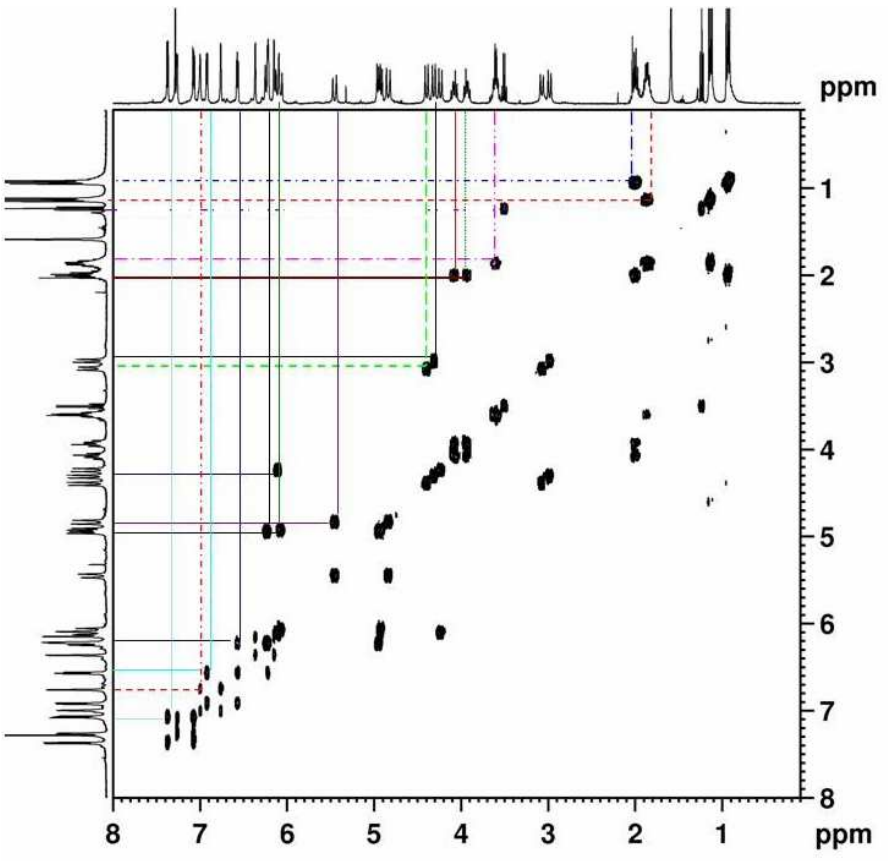

Figure S40. ^{1}H-^{1}H COSY NMR spectrum of complex **3** in $CDCl_3$ at 298 K.

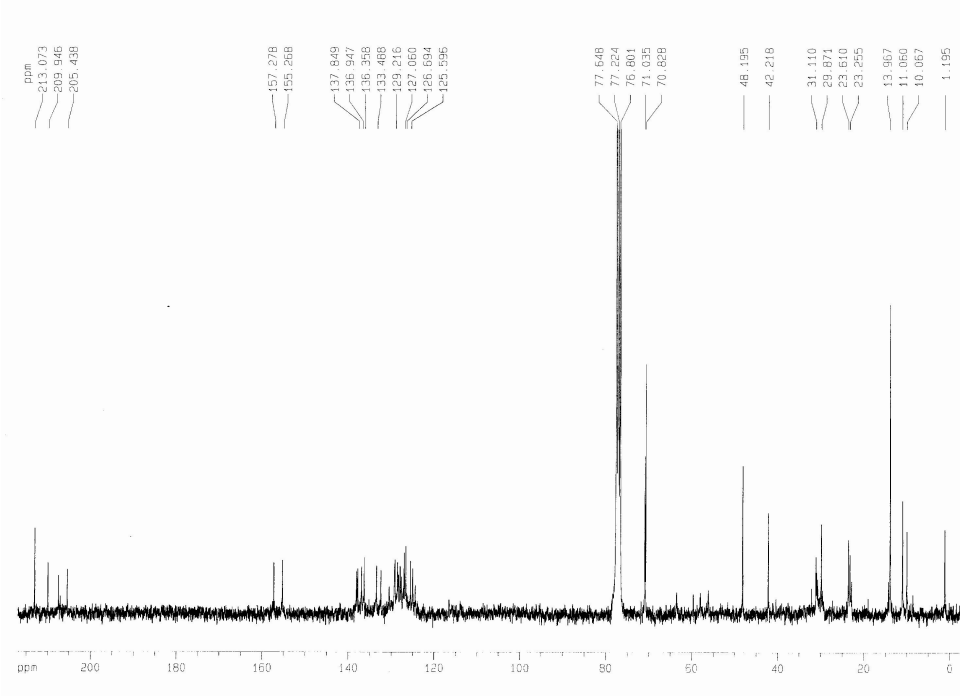

Figure S41. ^{13}C NMR spectrum of complex **3** in $CDCl_3$ at 298 K.

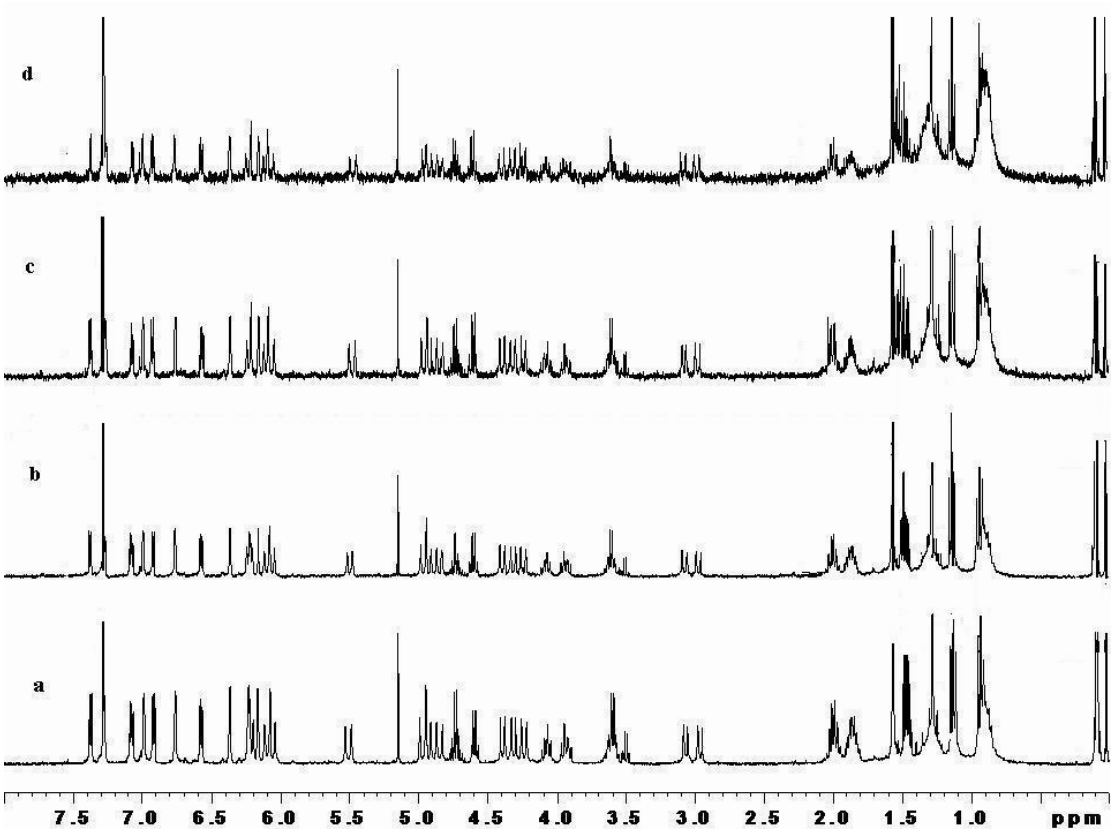

Figure S42. ^{1}H NMR spectra of complex **3** at different concentrations in $CDCl_3$ (a, 5.21 mM; b, 2.58 mM; c, 1.25 mM; d, 0.52 mM) at 298 K.

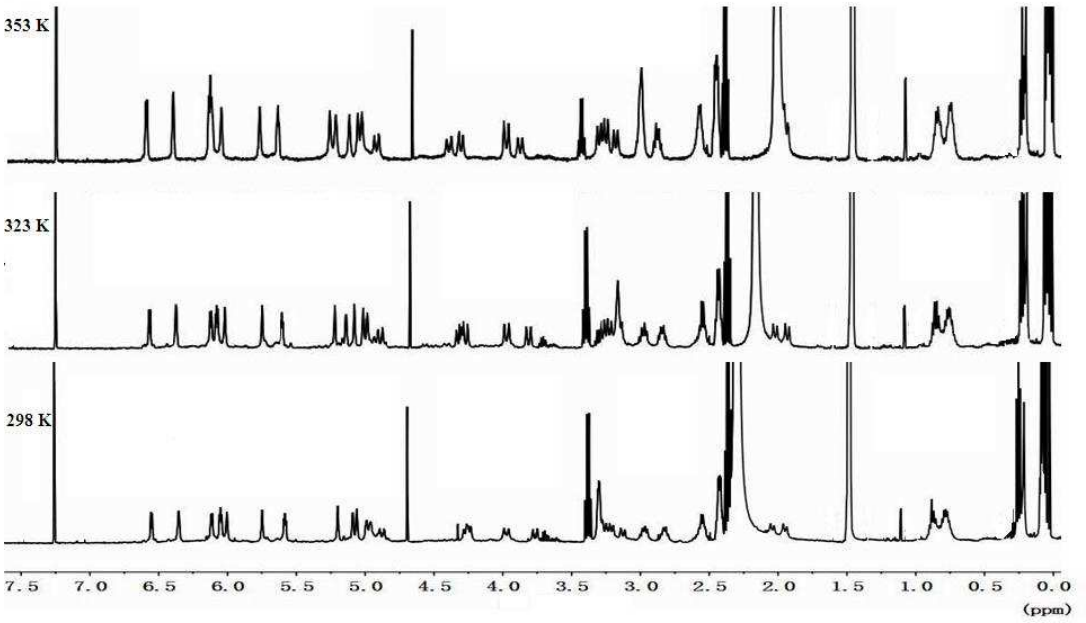

Figure S43. Variable-temperature ^{1}H NMR spectra of complex **3** in $CDCl_3$/d_6-DMSO (1:2, v/v) (Bottom to top: 298 K, 323 K and 353 K) (500 MHz).

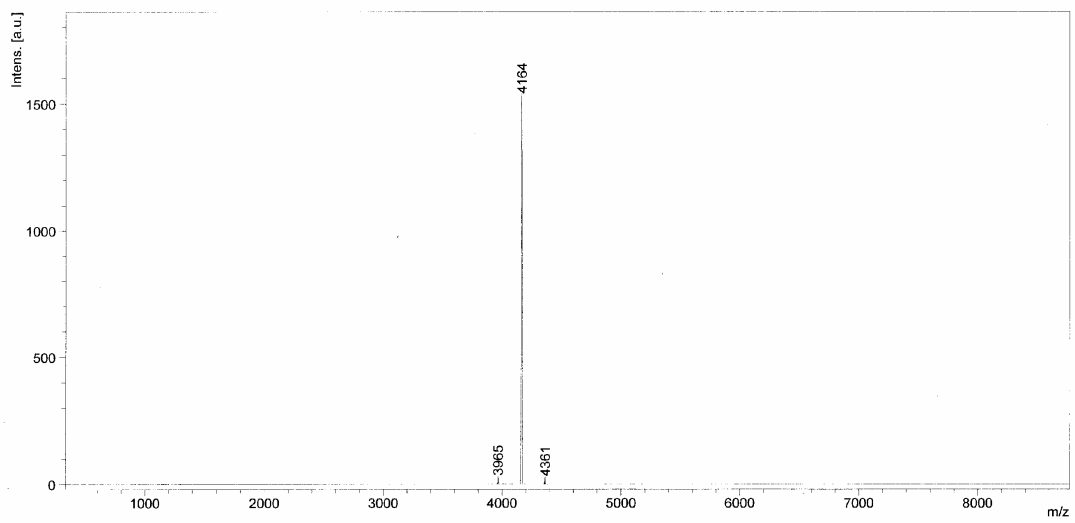

Figure S44. MALDI-TOF-MS spectrum of complex **3** in $CHCl_3$ at 298 K, m/z = 4361, $[Au_8L_2+H^+]^+$; 4164, $[Au_7L_2+2H^+]^+$; 3965, $[Au_6L_2+3H^+]^+$.

S3. X-Ray crystallography of complexes **1-3**

X-Ray diffraction data of the crystals of complex **1-3** were collected using synchrotron radiation (λ = 0.80010 Å) via the 3W1A in the IHEP with the approval of the Beijing Synchrotron Research Radiation Facility (BSRF). The diffraction data reduction and integration were performed by the HKL2000 software. Positions of the Au atoms and most of the non-hydrogen atoms were found using the direct methods program in the Bruker SHELXTL software package.[3-5] All hydrogen atoms were placed in calculated positions in the final structure refinement. Crystal structure refinement data are given in Table S1. The selected geometric parameters are shown in Tables S2-S4.

Table S1. Crystal structure determination data for complex **1-3**

Complex	**1**	**2**	**3**
Formula	$C_{304}H_{320}Au_{16}N_{16}O_{16}S_{32}$	$C_{160}H_{176}Au_8N_8O_8S_{16}$	$C_{277}H_{295}Au_{16}Cl_2N_{18}O_{16}S_{48}$
Fw	8631.14	4427.78	8893.97
Temperature (K)	120	120	120
Cryst syst	Orthorhombic	Monoclinic	Triclinic
Space group	Aba2 (No: 41)	$P2_1/n$ (No: 14)	$P\bar{1}$
a (Å)	36.0360 (10)	26.510(2)	21.957(4)
b (Å)	21.7320(10)	39.7900(10)	27.821(6)
c (Å)	41.308 (3)	39.011(3)	28.369(6)
α (°)	90	90	75.91(3)
β (°)	90	105.588(3)	72.76(3)
γ (°)	90	90	76.36(3)
V ($Å^3$)	32350 (3)	39637(4)	15800.6
Z	4	8	2
ρcalcd (gm^{-3})	1.772(1)	1.484	1.869
Total no.of data	40114	147982	22161
No. of unique data	21888	73534	33075
No. of parameters refined	1702	3605	3318
R_1 [I>2sigma(I)]	0.0427	0.0645	0.1103
wR_2	0.0958	0.1623	0.3201

Table S2. Selected bond distances (Å) for complex **1**.

	Bond Dist. (Å)		Bond Dist. (Å)
Au1-Au2	2.7771	Au5-Au6	2.767(7)
Au1-S1	2.316(3)	Au5-S5	2.315(3)
Au1-S9	2.334(3)	Au5-S13	2.404(3)
Au2-S2	2.365(3)	Au6-Au7	2.907(7)
Au2-S10	2.295(3)	Au6-S6	2.264(3)
Au3-Au4	2.799(6)	Au6-S14	2.253(3)
Au3-S3	2.299(3)	Au7-Au8	2.763(6)
Au3-S11	2.299(3)	Au7-S7	2.287(3)
Au4-S4	2.309(3)	Au7-S15	2.302(3)
Au4-S12	2.307(3)	Au8-S8	2.309(3)
Au4-Au4a	2.997(6)	Au8-S16	2.316(3)

Table S3. Selected bond distances (Å) for complex **2**.

	Bond Dist. (Å)		Bond Dist. (Å)
Au1-Au2	2.7733(4)	Au8-S16	2.2579(19)
Au1-S1	2.2917(2)	Au9-Au10	2.7818(4)
Au1-S9	2.2654(17)	Au10-S26	2.2725(17)
Au2-S2	2.2933(18)	Au10-S18	2.3009(17)
Au2-S10	2.2934(18)	Au10-Au11	3.0778(5)
Au2-Au3	3.1007(5)	Au11-S27	2.2623(16)
Au3-S3	2.2497(17)	Au11-S19	2.2739(16)
Au3-S11	2.2859(17)	Au11-Au12	2.7789(5)
Au3-Au4	2.7743(4)	Au12-S20	2.2793(18)
Au4-S4	2.2604(17)	Au12-S28	2.3112(17)
Au4-S12	2.2795(17)	Au13-S21	2.2579(17)
Au5-Au6	2.7644(4)	Au13-S29	2.2979(16)
Au5-S5	2.2487(17)	Au13-Au14	2.7651(4)
Au5-S13	2.2558(16)	Au14-S30	2.2817(17)
Au6-Au7	2.9813(4)	Au14-S22	2.3018(16)
Au6-S6	2.2849(18)	Au14-Au15	2.9702(4)
Au6-S14	2.3074(18)	Au15-S23	2.3053(19)
Au7-Au8	2.7631(4)	Au15-S31	2.3123(18)
Au7-S7	2.3131(18)	Au15-Au16	2.7530(4)
Au7-S15	2.2900(19)	Au16-S24	2.2835(17)
Au8-S8	2.2932(18)	Au16-S32	2.2886(18)

Table S4. Selected bond distances (Å) for complex **3**.

	Bond Dist. (Å)		Bond Dist. (Å)
Au1-Au2	2.802(2)	Au8-S4(2)	2.308(8)
Au1-S1(1)	2.31(1)	Au9-Au10	2.789(2)
Au1-S8(2)	2.32(1)	Au9-S1(3)	2.306(7)
Au1-Au16	3.076(2)	Au9-S1(4)	2.313(8)
Au2-Au3	2.956(2)	Au10-Au11	2.956(2)
Au2-S2(1)	2.29(1)	Au10-S2(3)	2.296(9)
Au2-S7(2)	2.27(1)	Au10-S2(4)	2.294(9)
Au3-Au4	2.801(2)	Au11-Au12	2.781(2)
Au3-S3(1)	2.28(1)	Au11-S3(3)	2.307(9)
Au3-S6(2)	2.27(1)	Au11-S3(4)	2.284(9)
Au4-S4(1)	2.281(8)	Au12-S4(3)	2.29(1)
Au4-S5(2)	2.315(8)	Au12-S4(4)	2.29(1)
Au4-Au12	3.203(2)	Au12-Au4	3.203(2)
Au5-Au6	2.776(3)	Au13-Au14	2.808(2)
Au5-S5(1)	2.289(9)	Au13-S8(3)	2.302(7)
Au5-S1(2)	2.289(9)	Au13-S8(4)	2.295(7)
Au6-Au7	2.960(2)	Au14-Au15	2.973(2)
Au6-S6(1)	2.297(8)	Au14-S7(3)	2.273(9)
Au6-S2(2)	2.32(1)	Au14-S7(4)	2.285(8)
Au7-Au8	2.788(2)	Au15-Au16	2.808(2)
Au7-S7(1)	2.298(9)	Au15-S6(3)	2.29(1)
Au7-S3(2)	2.292(8)	Au15-S6(4)	2.31(1)
Au8-Au9	2.971(2)	Au16-S5(3)	2.32(1)
Au8-S8(1)	2.305(8)	Au16-S5(4)	2.317(9)
		Au16-Au1	3.076(2)

S4. Photophysical data and excitation spectra of complexes **1-3**

Table S5. Emission data for complexes **1-3**

Complex	Medium (T/K)	Emission λ / nm (τ_0/μs)	Φ_{lum}[a]
1	CH_2Cl_2 (298)	559 (1.04)	2.75 x 10^{-3}
	Solid (298)	614 (4.52)	
	Solid (77)	624 (6.32)	
	Glass (77)	537 (3.35)	
2	CH_2Cl_2 (298)	561 (1.76)	5.72 x 10^{-3}
	Solid (298)	non-emissive	
	Solid (77)	544 (5.58)	
	Glass (77)	518 (2.62)	
3	CH_2Cl_2 (298)	567 (1.23)	3.75 x 10^{-3}
	Solid (298)	non-emissive	
	Solid (77)	644 (6.78)	
	Glass (77)	531 (2.12)	

[a] Luminescence quantum yield, measured at room temperature using quinine sulfate in 1.0 N H_2SO_4 as reference

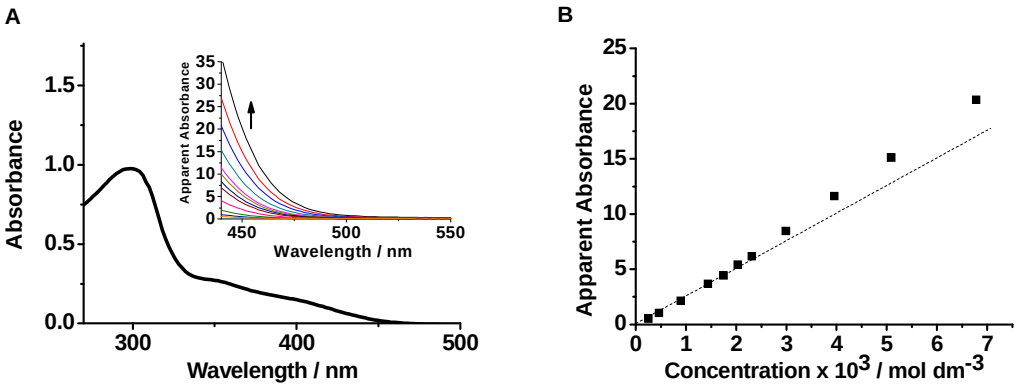

Figure S45. (A) UV-Vis absorption spectrum of complex **3** in dichloromethane. Inset: UV-Vis absorption spectral changes of **3** in dichloromethane as the concentration increases from 2.52 x 10^{-4} to 6.78 x 10^{-3} M. The apparent absorbance values have been corrected to a 1-cm path-length equivalence. (B) A plot of absorbance at 450 nm as a function of concentration for complex **3**. Experimental (■) and theoretical (---) fit to Beer's law.

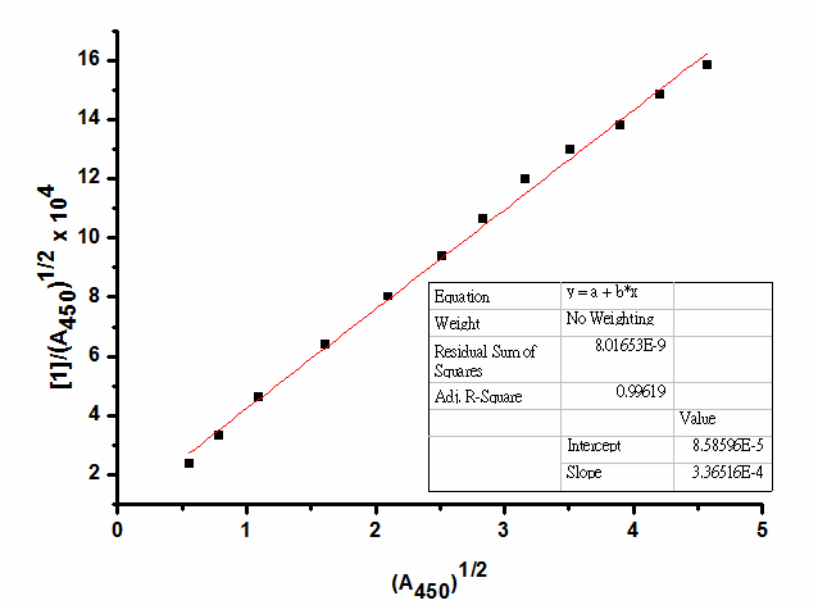

Figure S46. The dimerization plot for a monomer-dimer equilibrium for complex **1**.

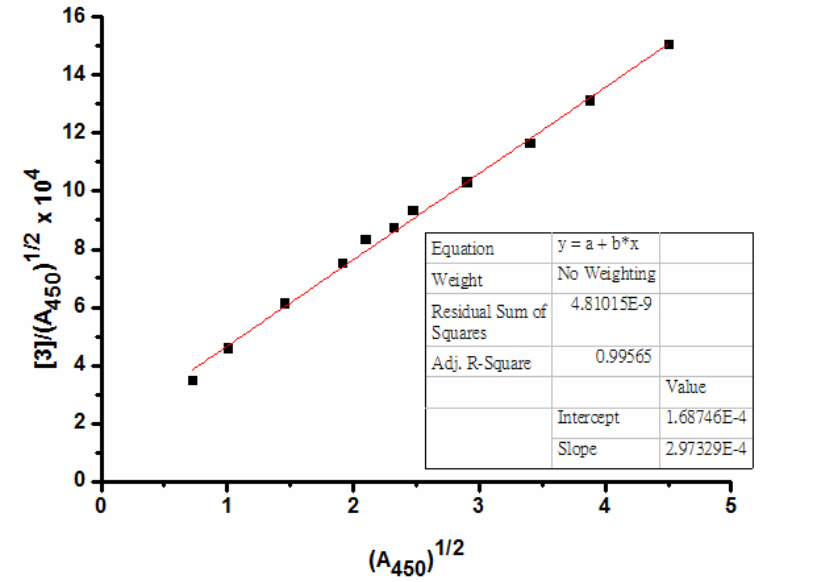

Figure S47. The dimerization plot for a monomer-dimer equilibrium for complex **3**.

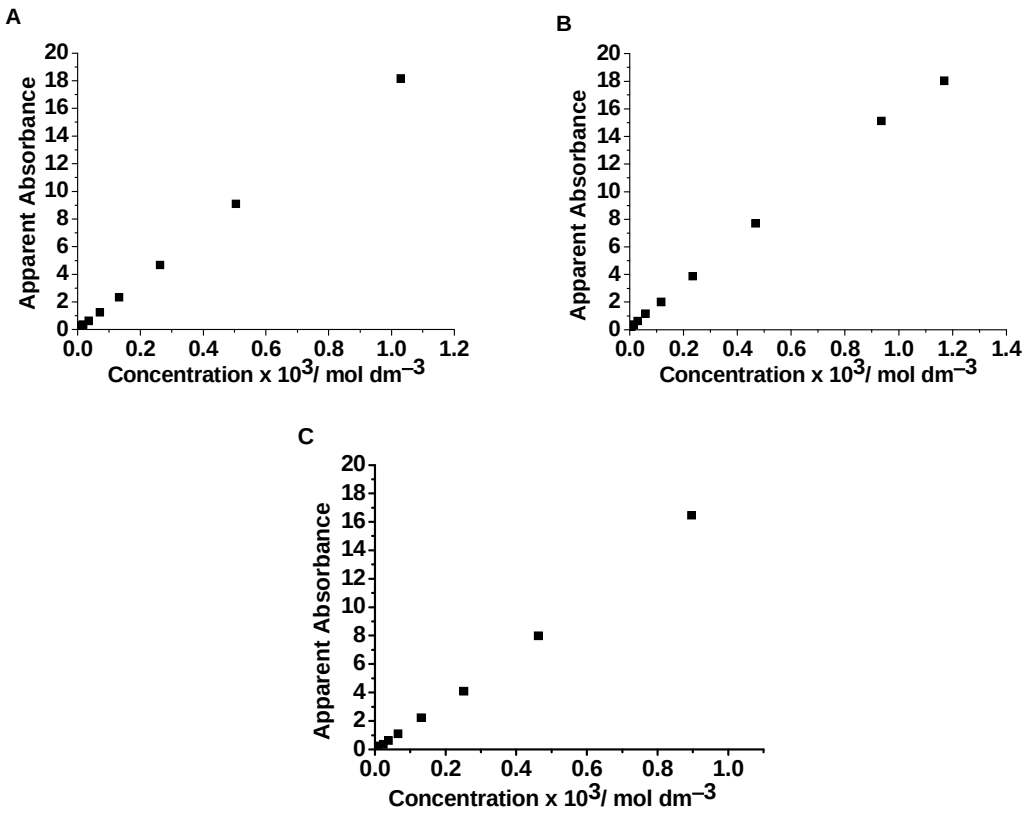

Figure S48. A plot of absorbance at 400 nm as a function of concentration for (A) complex **1** increases from 4.45×10^{-6} to 1.03×10^{-3} M; (B) complex **2** increases from 1.83×10^{-6} to 1.03×10^{-3} M; (C) complex **3** increases from 1.77×10^{-6} to 8.96×10^{-4} M.

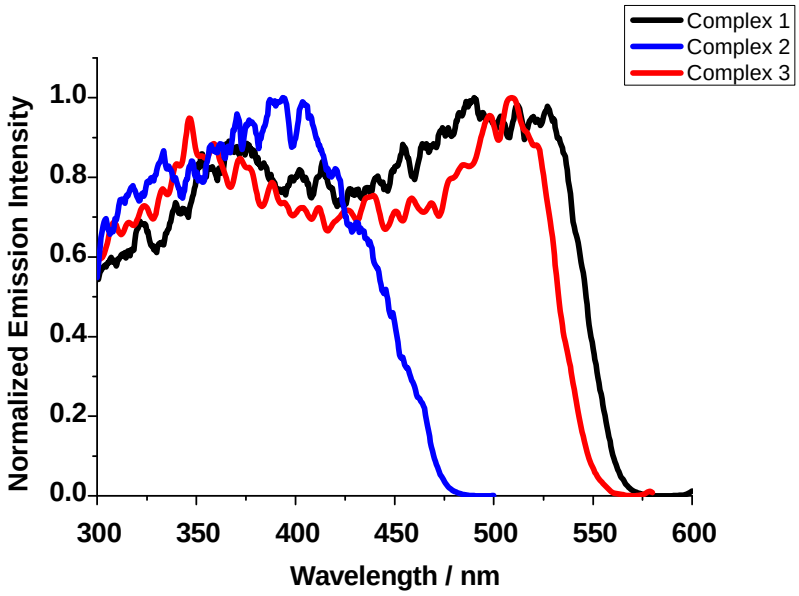

Figure S49. Excitation spectra of complexes **1-3** monitored at 700 nm, 600 nm and 710 nm, respectively.

S5. Host-guest interaction driven luminescent chemosensing for silver ions and photo-switchable behavior within supramolecular cages.

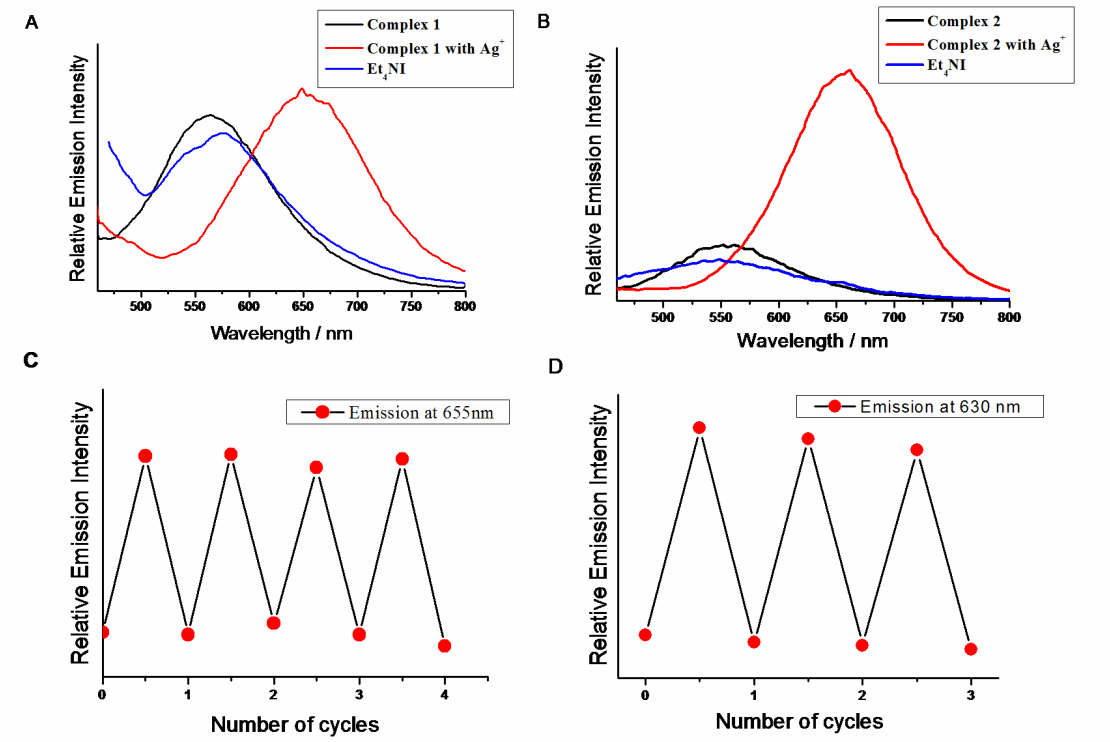

Figure S50. Reversible photo-switching of emission spectral changes upon titration with Ag^{+} and I^{-} (tetraethylammonium iodide) of (A) complex **1** and (B) complex **2**, both measured in CH_2Cl_2-CH_3CN (20:1 v/v) solution (λ_{ex} = 430 nm). Reversible emission changes of the complex as photo-switching sensors from single cage to cage with silver ions recycled using tetraethylammonium iodide for (C) **1** at 655 nm, and (D) **2** at 660 nm.

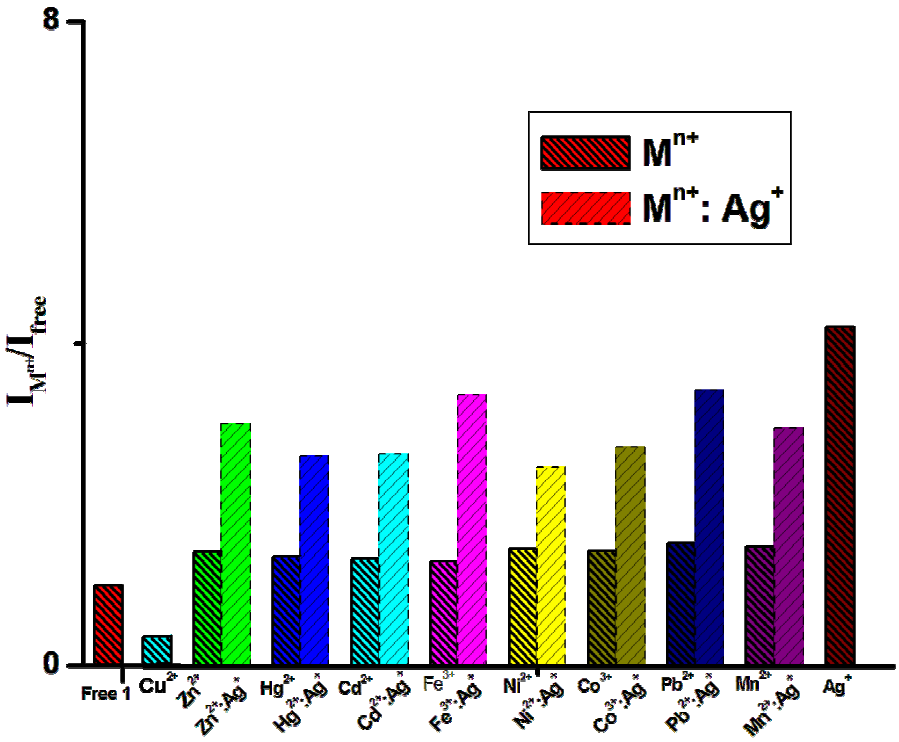

Figure S51. Emission intensity changes of complex **1** (2×10^{-5} mol/L) in the presence of various metal ions (10 equiv.) (M^{n+} = Zn^{2+}, Cd^{2+}, Hg^{2+}, Fe^{3+}, Ni^{2+}, Co^{2+}, Pb^{2+} and Mn^{2+}; λ_{em}= 550 nm, λ_{ex}= 430 nm) and competitive binding with metal ions (upon titration with 10 equiv mixed solution of $AgNO_3$ and metal ion with a Ag^+ : M^{n+} ratio of 1:1, both measured in $CHCl_3$-CH_3CN (20:1 v/v) solution (λ_{em}= 620 nm, λ_{ex}= 430 nm)).

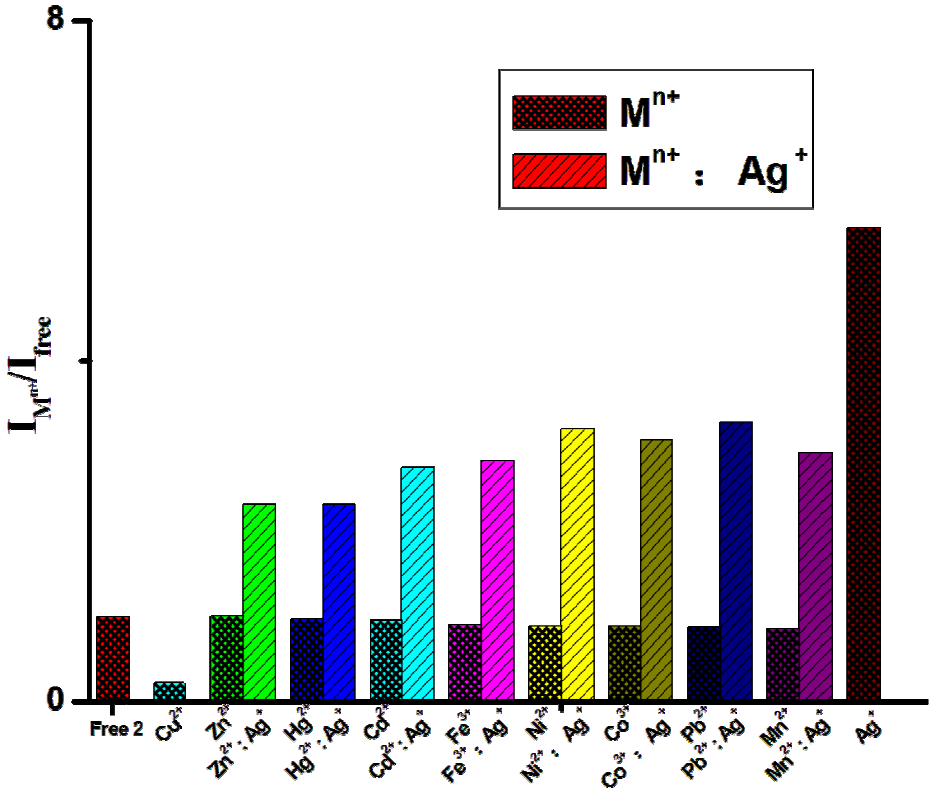

Figure S52. Emission intensity changes of complex **2** (2×10^{-5} mol/L) in the presence of various metal ions (10 equiv.) (M^{n+} = Zn^{2+}, Cd^{2+}, Hg^{2+}, Fe^{3+}, Ni^{2+}, Co^{2+}, Pb^{2+} and Mn^{2+}; λ_{em}= 554 nm, λ_{ex}= 430 nm) and competitive binding with metal ions (upon titration with 10 equiv mixed solution of $AgNO_3$ and metal ion with a Ag^+ : M^{n+} ratio of 1:1, both measured in $CHCl_3$-CH_3CN (20:1 v/v) solution (λ_{em}= 620 nm, λ_{ex}= 430 nm)).

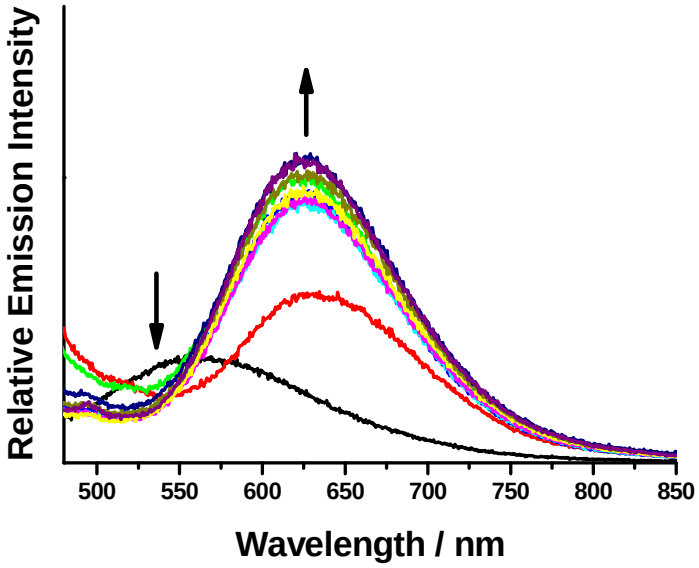

Figure S53. Emission spectral changes of complex **3** $\{Au_8L_2\}_n$ titrated with $AgPF_6$ (from 0-2 equiv) in $CHCl_3$-CH_3CN (20:1 v/v) solution with 1 mM $^nBu_4N(PF_6)$ (λ_{ex}= 430 nm).

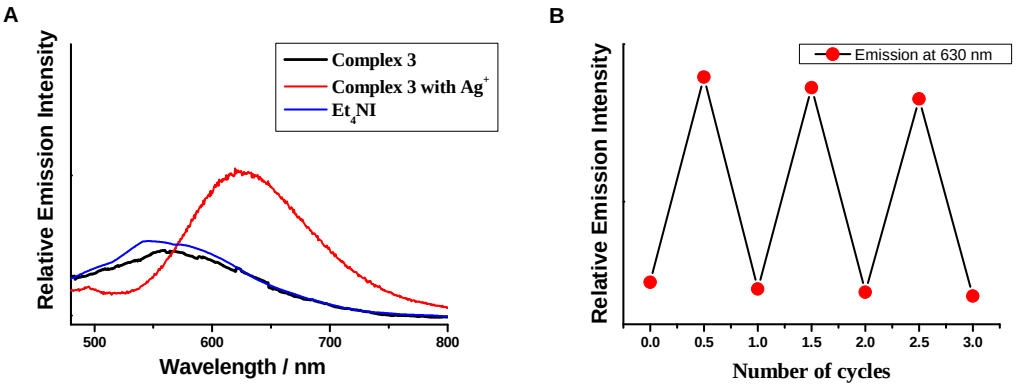

Figure S54. Reversible photo-switching of emission spectral changes upon titration with Ag^+ and I^- (tetraethylammonium iodide) of complex **3** measured in CH_2Cl_2-CH_3CN (20:1 v/v) solution (λ_{ex} = 430 nm). Reversible emission changes of the complex as photo-switching sensors between complex **3** and **3**•Ag^+ at 630 nm.

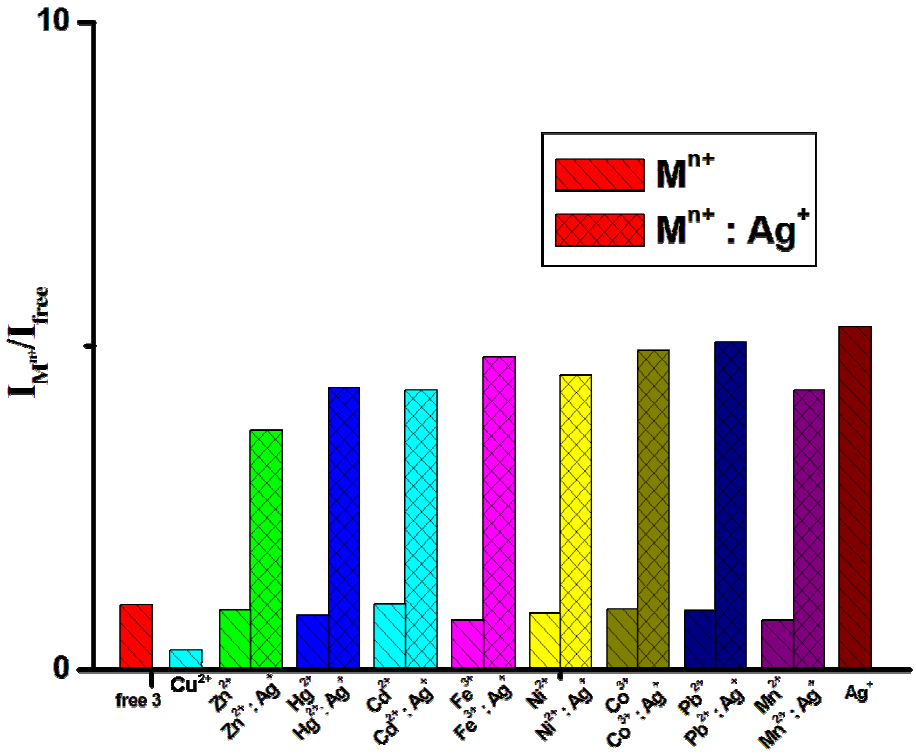

Figure S55. Emission intensity changes of complex **3** (2×10^{-5} mol/L) in the presence of various metal ions (10 equiv.) (M^{n+} = Zn^{2+}, Cd^{2+}, Hg^{2+}, Fe^{3+}, Ni^{2+}, Co^{2+}, Pb^{2+} and Mn^{2+}; λ_{em}= 550 nm, λ_{ex}= 430 nm) and competitive binding with metal ions (upon titration with 10 equiv mixed solution of $AgNO_3$ and metal ion with a Ag^+ : M^{n+} ratio of 1:1, both measured in $CHCl_3$-CH_3CN (20:1 v/v) solution (λ_{em}= 630 nm, λ_{ex}= 430 nm)).

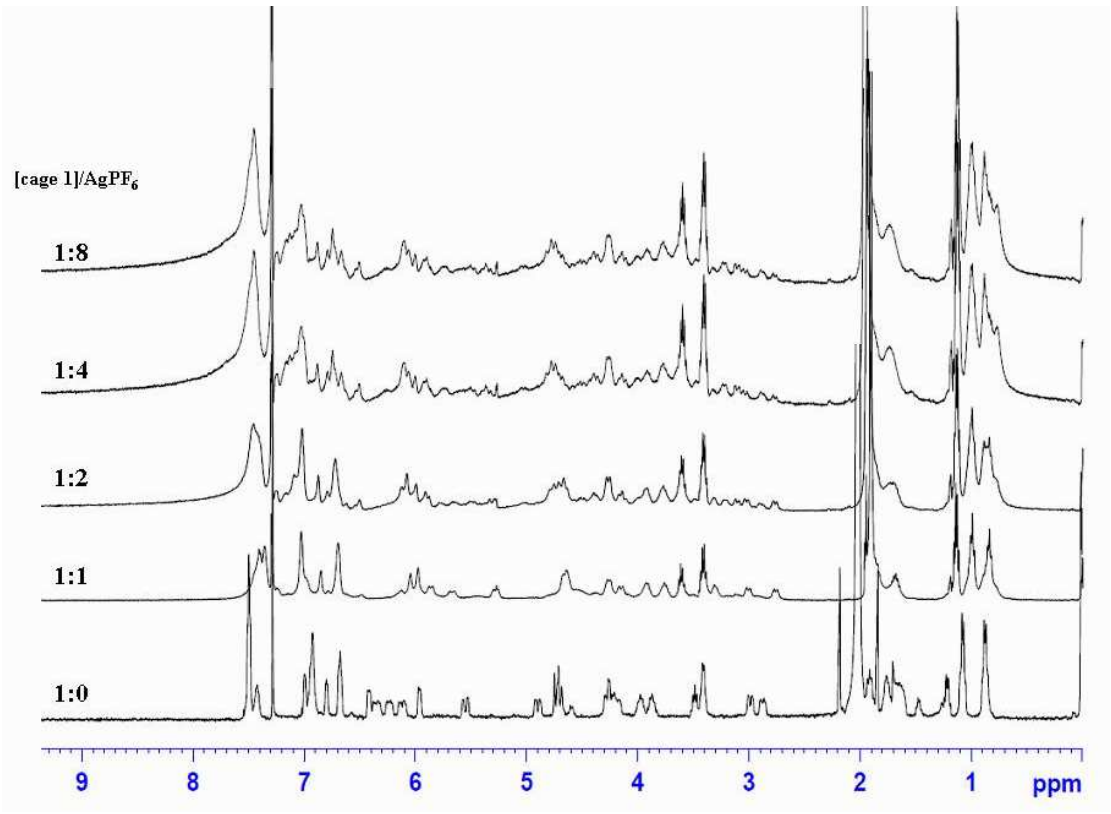

Figure S56. ^{1}H NMR spectra of complex **1** titrated with $AgPF_6$ (0-6 equiv. in CD_3CN solution) in $CDCl_3$-CD_3CN (10:1 v/v) at 298 K.

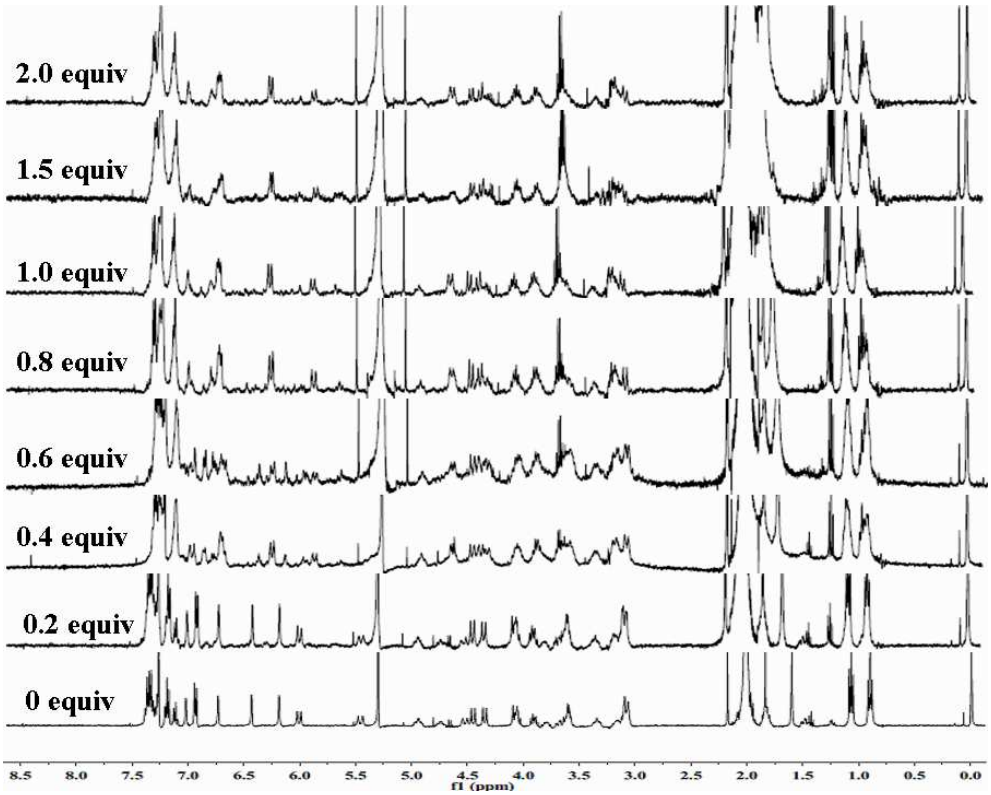

Figure S57. ^{1}H NMR spectra of complex **2** titrated with $AgPF_6$ (0-2 equiv. in CD_3CN solution) in $CDCl_3$-CD_3CN (20:1 v/v) at 298 K.

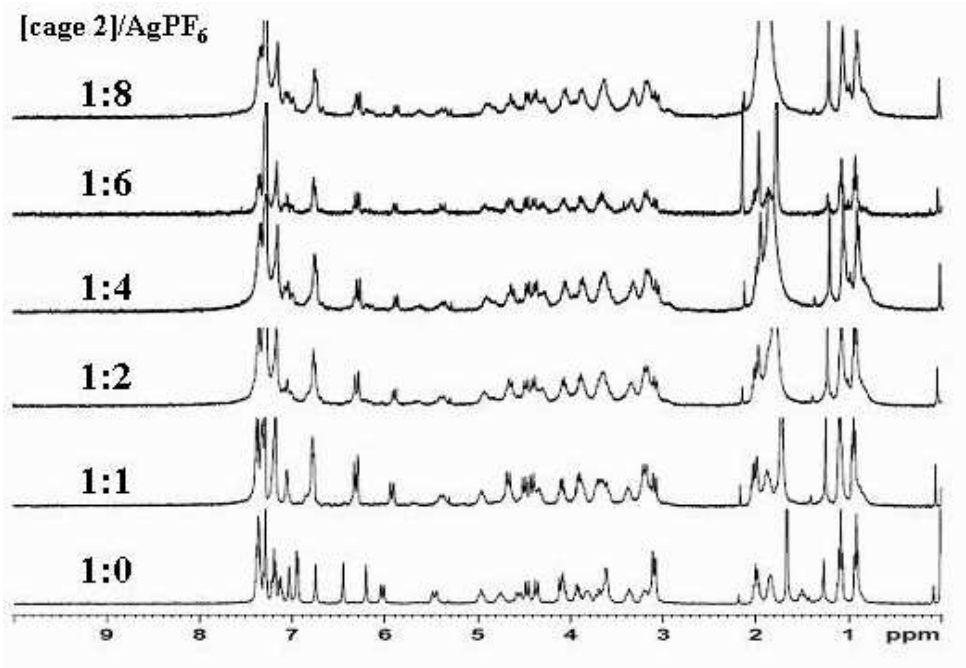

Figure S58. ^{1}H NMR spectra of complex **2** titrated with $AgPF_6$ (0-8 equiv. in CD_3CN solution) in $CDCl_3$-CD_3CN (20:1 v/v) at 298 K.

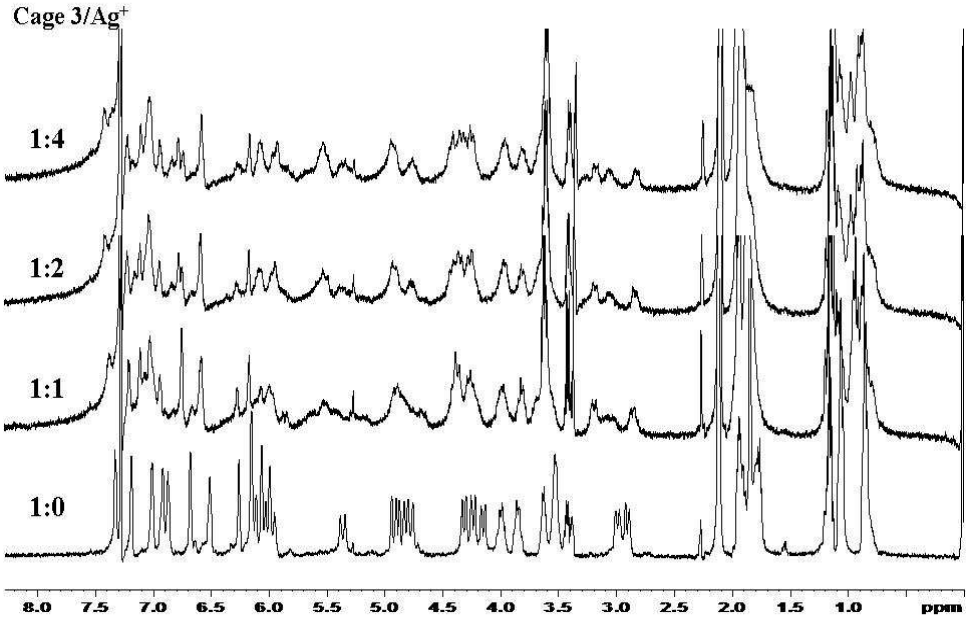

Figure S59. ^{1}H NMR spectra of complex **3** titrated with $AgPF_6$ (0-4 equiv. in CD_3CN solution) in $CDCl_3$-CD_3CN (20:1 v/v) at 298 K.

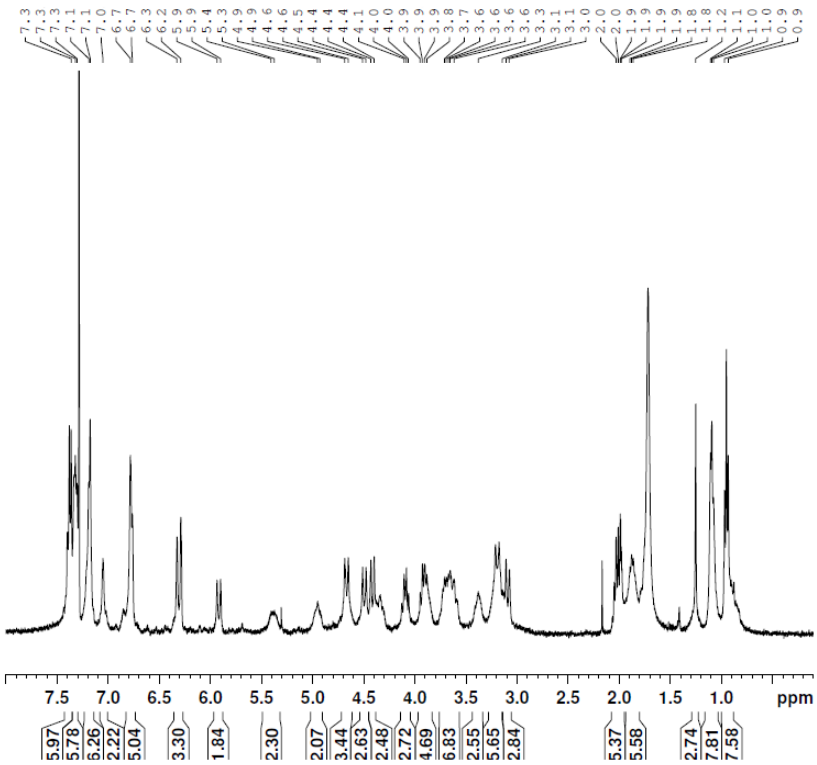

Figure S60. ^{1}H NMR spectrum of complex **2**•AgOTf in $CDCl_3$-CD_3CN (50:1 v/v) at 298 K.

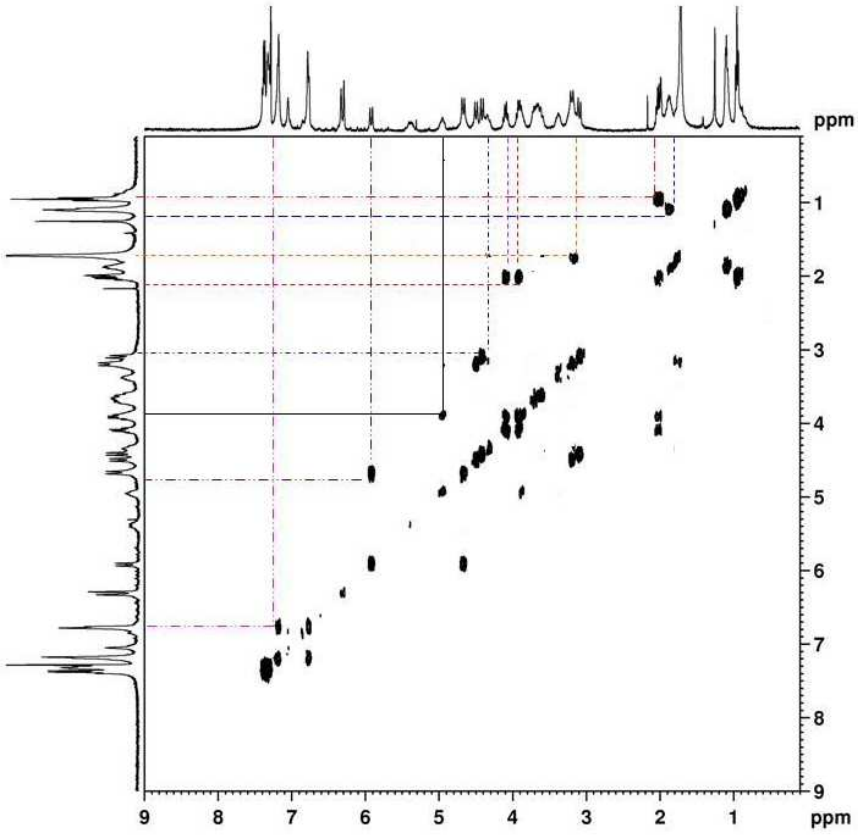

Figure S61. ^{1}H-^{1}H COSY NMR spectrum of the complex **2**•Ag^{+} in $CDCl_3$-CD_3CN (50:1 v/v) at 298 K.

S6. References

[1] a) Sansonea, F.; Barbosoa, S.; Ungaro, R. *Eur. J. Org. Chem.* **1998**, 897.

b) Gutsche, C. D.; Pagoria, P. F. *J. Org. Chem.* **1985**, *50*, 5795.

c) Arduini, A.; Fabbi, M.; Mantovani, M.; Mirone, L.; Pochini, A.; Secchi, A.; Ungaro. R. *J. Org. Chem*. **1995**, *60*, 1454.

[2] a) Yu, S. Y.; Zhang, Z. X.; Cheng, E. C. C.; Li, Y. Z.; Yam, V. W. W.; Huang, H. P.; Zhang, R. B. *J. Am. Chem. Soc.* **2005,** *127*, 17994.

b) Yu, S. Y.; Sun, Q. F.; Lee, T. K. -M.; Cheng, E. C. -C.; Li, Y. Z.; Yam, V. W.-W. *Angew. Chem. Int. Ed.* **2008**, *47*, 4551.

c) Sun, Q. -F.; Lee, T. K. -M.; Li, P. -Z.; Yao, L. -Y.; Huang, J. -J.; Huang, J.; Yu, S. -Y.; Li, Y. -Z.; Yam, V. W. -W. *Chem. Commun.* **2008**, *43*, 5514.

d) Cotton, F. A.; Lei, P.; Lin, C.; Murillo, C.A.; Wang, X.; Yu, S. -Y.; Zhang, Z.-X. *J. Am. Chem. Soc.* **2004**, *126*, 1518.

[3] Sheldrick, G. M. SHELXS-97 (Univ. Göttingen, 1990).

[4] Sheldrick, G. M. SHELXL-97 (Univ. Göttingen, 1997).

[5] Spek, A. & van der Sluis, P. BYPASS: an effective method for the refinement of crystal structures containing disordered solvent regions. Acta Crystallogr. A 46, 194 – 201 (1990).